Fabrication and Characterization of Polyethersulfone Nanocomposite Membranes for the Removal of Endocrine Disrupting Micropollutants from Wastewater. Mechanisms and Performance

G. Kaminska[1], J. Bohdziewicz[1], J.I. Calvo[2], P. Prádanos[2], L. Palacio[2], A. Hernández[2*]

[1]. Institute of Water and Wastewater Engineering, Faculty of Environmental Engineering and Energy, Silesian University of Technology, 44-100 Gliwice, Konarskiego 18 Str. Poland.

[2]. Grupo de Superficies y Materiales Porosos (SMAP, UA-UVA-CSIC), Dpto. de Física Aplicada, Facultad Ciencias, Universidad de Valladolid, 47071 Valladolid, Spain.

Abstract

The addition of carbon nanotubes to improves the removal and adsorption of endocrine disrupting micropollutants (bisphenol A and nonylphenol). Increasing the SWCNT (single walled carbon nanotubes) content increases removal and diminishes reversible and irreversible fouling.

The isoelectric point of the SWCNT containing membranes decreases when the content of nanotubes increases with more negative charges at alkaline pH. Because, the nanotube loaded membranes are also less hydrophilic and bisphenol and nonylphenol are hydrophobous, adsorption plays a key role in the removal of micropollutants. An increase in the transmembrane applied pressure decreases the removal and more steeply for the membranes containing more SWCNT.

Higher porosities, leading to higher water permeabilities, are also obtained for more loaded membranes. Too high SWCNT contents lead to a saturation and decrease of removal probably because high porosities lead to a decrease in adsorption due to both a decrease in the available surface and a sweeping action of convection through the membrane.

Key Words

Endocrine disrupting micropollutants, Carbon nanotubes, Nanocomposite membranes, Adsorption, Membrane characterization

(*) To whom correspondence should be addressed. E-mail: membrana@termo.uva.es.

1 Introduction

The modification of the membrane structure by carbon nanotubes is an interesting procedure in membrane technology. The nanotubes, incorporated within the structure of a membrane, play the role of a porous agent and sorbent. Such prepared nano-membrane has completely different structure and properties in comparison to conventional polymer membranes. In most cases, the incorporation of nanotubes within a membrane structure causes the overall increase of porosity of the membrane [1,2,3].

In these composite membranes, their surface expands due to strong interactions between polymer chains and nanoparticles. Moreover, this effect can be assumed to be caused by the tendency of nanotubes to the formation of aggregates giving an overall size significantly exceeding the size of typical individual nanoparticle [4]. Big nano-aggregates embedded in the polymer matrix can create macro-voids in the membrane structure and increase their permeability [2]. However, on the other hand, high concentration of nanomaterials can lead to a reversible decrease of membrane pore size. This is due to the significant increase of viscosity of the casting solution that slows down the penetration of non-solvent within the membrane structure during precipitation [5].

Thus, this it is very difficult to unequivocally determine the optimal concentration of nanomaterial in the polymer membrane to guarantee the highest permeability and selectivity. The proportion of nanomaterials in a membrane should be selected depending on both the kind of polymer and the properties of the nanomaterials but also on the characteristics of the membrane process to be used. Therefore, the selection of the most favorable concentration of nanomaterials in casting solution should be adjusted individually.

The nanotube-polymer hybrid membranes have, of course, some clear advantages because they improve, for example, mechanical properties and thermal stability. This is connected with the high mechanical strength of the nanotubes. It is also associated with their large surface area that interacts with the matrix and reduces the movement of the polymer chains [2].

With respect to the application of such nano-composite materials in pressure-driven membrane processes, the most important factors are the resulting hydrophilicity and the paired increase of the fouling resistance of membrane. The addition of nanomaterials functionalized with oxygen groups to the polymer membranes is a strategy to control fouling by modifying their hydrophilicity and also giving the membrane an electric charge [1,6]. The increase of zeta potential of the membrane enhances an electrostatic repulsion between some pollutants and membrane surface thus, that would be retained without approaching neither coating the pore or membrane surfaces [7].

Other researchers reported some properties of the polymer membranes that seem to be modified by nanomaterials. However, results are very often contradictory because, in fact, it is impossible to unequivocally and universally determine, from their characterization, what is the effect of the added nanotubes because their effect depends greatly on the properties of the original polymer. This is why, nanotube membranes should be better characterized in detail separately. Therefore, in this paper, the influence of carbon nanotubes on the structure and properties of polyethersulfone membranes is studied

Available data from the literature do not report removal of organic micro-pollutants using nano-membrane. The novelty of this work consists in the use of Polyethersulfone (PES) membranes filled with carbon nanotubes for the removal of micro-pollutants with estrogenic activity from synthetic wastewater.

2 Materials and methods

2.1 Chemicals

Carboxyl functionalized Single Walled Carbon Nanotubes (SWCNTs) were purchased from COCC (Chengdu, Sichuan, China). These nanotubes were synthesized by the chemical vapour deposition method and the raw product was purified using a mixture of HNO_3 and H_2SO_4 acids (data from manufacturer). The characteristics of the nanotubes as provided by the manufacturer are presented in Table 1. PES was supplied by BASF Company (Ludwigshafen, Germany). N,N-dimethylformamide, isopropanol (all analytically pure), acetonitrile and methanol for HPLC were purchased from Avantor Performance Materials (Central Valley, Pennsylvania, USA). Isobutanol (analytical grade) was supplied by Merck KGaA (Darmstadt, Germany). Potassium chloride, sodium hydroxide and hydrochloric acid were purchased from Sigma-Aldrich (St. Louis, Missouri, USA, now a subsidiary of Merck KGaA). Dextrane of a molecular weight of 40 kDa was also purchased from Sigma-Aldrich. Bisphenol-A (BPA) or 4,4'-(propane-2,2-diyl)diphenol and 4-Nonylphenol (4-(2,4-dimethylheptan-3-yl)phenol) (purity >99%) were purchased from Sigma Aldrich. The stock solutions of BPA and NP (4-Nonylphenol) were prepared with methanol (analytical standard). Deionised water was taken directly from Milli-Q water purification system (Millipore, Billerica, Massachusetts, USA, now a subsidiary of Merck KGaA).

Table 1. Characteristics of nanotubes.

2.2 Synthetic wastewater

A solution of synthetic wastewater was prepared to mimic municipal effluent containing estrogenic compounds. This was done by dissolving the following chemicals (mg/dm^3): bouillon: 2.5; peptones: 2.0; NH_4Cl: 3.5; NaCl: 1.5; $CaCl_2$: 5.0; $MgSO_4 \cdot 7H_2O$: 1.0; K_2HPO_4: 1.5; KH_2PO_4: 2.5 in deionised water. All substances were of analytical grade, purchased from Avantor Performance Materials (Central Valley, Pennsylvania, USA). Sufficient volumes of BPA and NP stock solutions were added to achieve a concentration of 100 $\mu g/dm^3$ in wastewater. BPA hormone-like properties that raise concern about its suitability in some consumer products and food containers and NP is considered to be an endocrine disruptor due to its ability to mimic estrogen and in turn disrupt the natural balance of hormones in affected organisms. pH of this synthetic wastewater varied from 6.9 to 7.4. The properties of selected micropollutants are shown in Table 2.

Table 2. Characteristics of compounds.

2.3 Preparation of PES/nano-composite membranes

Pristine polymeric membranes contained 16 wt% polyethersulfone (PES) and 84wt% N,N-dimethylformamide (DMF). The casting solution for nanocomposite membranes consisted of 16 wt% PES-SWCNT and 84 wt% DMF. The loading of SWCNT in 16 wt% PES-SWCNT was kept as 0.025; 0.05; 0.1 and 0.5 wt%. Thus, the ratio between PES and SWCNT was at the levels of 99.975:0.025; 99.95:0.05; 99.9:0.1 and 99.5:0.5. The membranes were named as: PES (membrane without nanotubes); PES 0.025%SWCNT; PES 0.05%SWCNT; PES 0.1%SWCNT; PES 0.5%SWCNT.

Polymeric flat membranes were prepared via the phase inversion method. To prepare the nanocomposite membranes, firstly, an appropriate amount of carbon nanotubes was added to DMF. This mixture was subjected to ultrasonication (30 min), in order to minimize the aggregation effects of nanotubes. After that, a suitable amount of PES was put in the mixture with the nanotubes and DMF. Casting solution was intensively stirred for 12 h at 45 ^{o}C to assure a good homogeneization and then degassed in order to remove air bubbles.

Subsequently, the membranes were cast using a doctor blade mechanism as 150 μm films onto a glass plate and immediately immersed into the coagulation bath (deionised water/isopropanol 90/10, v/v) at 15±1^{o}C. After membrane precipitation, the membranes were stored in deionised water at 4 ^{o}C for 24 h to ensure complete phase separation.

2.4 Characterization of PES/nano-composite membranes

2.4.1 Liquid-liquid displacement porometry

The pore size distribution and porosity of our membranes were measured by means of liquid-liquid displacement porometry (LLDP). Following this method, membranes were soaked in a wetting liquid, which were subsequently pushed out by an immiscible liquid. The wetting liquid was an aqueous-rich phase while the immiscible liquid was an alcohol-rich phase. They were obtained by putting degased and deionized water along with isobutanol (350/150, v/v) in a separating funnel and shaking it intensively. Then, the mixture was stood overnight for separating both phases. The apparatus used in the analysis was completely automated. A detailed description of LLDP theory and experimental procedure can be seen elsewhere [8].

The LLDP method is based on the measurements of pressure and flow through the membrane, consequently leading to the calculation of pore radius opened at the given applied pressure. The pore radius (r) was calculated by the Young-Laplace equation:

$$r = \frac{2\gamma}{\Delta p}\cos\theta \qquad (1)$$

Δp is the transmembrane pressure, γ is the interfacial tension between the two liquids and Θ the contact angle at the corresponding interface between displacing

and displaced liquids and the membrane material. In our case we can take the contact angle as zero (Equation (1) is then called Cantor's equation) and γ = $1.9 \cdot 10^{-3}$ N/m. Assuming cylindrical pores, the Hagen-Poiseuille equation can be used to correlate the volume flow (J_{Vd}) of the displacing fluid and the number of pores (n), having a given pore radius. For each pressure value (Δp_i), the corresponding volume flow measured is correlated with the number of pores thus opened by:

$$J_{Vd} = \sum_{k=1}^{i} \frac{n_k \pi r_k^4 \Delta p_i}{8 \eta_d l} \quad (2)$$

η_d is the dynamic viscosity of the displacing fluid and l the pore length, which refers to the active layer thickness of the membrane in the case of asymmetric membranes. By raising the pressure stepwise, corresponding pore radius and flow values are revealed and the total permeability of the membrane can be acquired. Moreover, molecular weight cut off was estimated from LLDP data using a procedure previously published [9].

2.4.2 Retention tests

A dead-end filtration set-up was used to perform retention tests. The device consisted essentially in three elements: a stirred cell, a pressure providing gas system and a vessel to collect the permeate. The stirred cell used was the HP4750 stirred cell from Sterlitech (Kent, Washington state, USA). The cell leaves an active membrane area of 14.6 cm^2. A membrane disk is held between the reservoir cell for the liquid feed and a stainless steel porous support disk. The flow through the membrane is driven by a pressurized air cylinder, which is controlled by a DHP 240-50-10 Air-Liquide pressure regulator. The reservoir cell is stirred by a Teflon coated magnetic stir bar (length d_{sb} = 22.00 ± 0.05 mm) on an Agimatic-N stirrer, which controls the rotation velocity of the bar. Some more detailed description of this device can be seen elsewhere [10]. In this case we used a feed reservoir of 300 mL with a dextrane concentration of 0.99 g/L permeating at 0.5 bar with stirring at 1600 r.p.m.

The Peclet number (*Pe'*) is the ratio of the convective to diffusive contributions to the permeation and can be defined as:

$$Pe' = \frac{K_c' J_V}{K_d' D_s} \left(\frac{\Delta x}{A_k} \right) \quad (3)$$

Δx in the thickness of the active layer of the membrane, A_k is its surface porosity (open area per unit of total area), D_s is the diffusivity of the solute, J_V is the volume flux through the membrane and K'_c and K'_d are the corrected hindrance factor for the convection and diffusion, respectively. The retention of the membrane, or true retention coefficient, can be expressed as a function of the pore radius [11] for each J_V as:

$$R = 1 - \frac{C_p}{C_m} = 1 - \frac{K_c' \phi}{1 - \left(1 - K_c' \phi\right) e^{-Pe'}} \qquad (4)$$

C_p is the concentration of the permeate while C_m is the concentration on the membrane at the feed-membrane side; and ϕ the partitioning coefficient. Different correlations have been proposed in the literature for the hindrance factors and on how to evaluate them from $\lambda = r_s / r_p$ (the ratio of solute to pore radii). Assuming cylindrical pores $\phi = (1 - \lambda)^2$.

A careful revision was done by Dechadilok and Deen [12]. They also studied and presented a way of introducing the effects of the pressure gradient in these hindrance factors. Expressions for K_c and K_d used in this work are those proposed in the cited work by Dechadilok and Deen for cylindrical pores:

$$\left.\begin{aligned} K_d &= \frac{1}{1-\lambda^2}\left(1 + \frac{9}{8}\lambda \ln\lambda - 1.5603\lambda + 0.52815\lambda^2 + 1.9152\lambda^3 - 2.8190\lambda^4 + \right. \\ &\qquad \left. + 0.27078\lambda^5 + 1.10115\lambda^6 - 0.43593\lambda^7\right) \\ K_c &= \frac{1 + 3.867\lambda - 1.907\lambda^2 - 0.834\lambda^3}{1 + 1.867\lambda - 0.741\lambda^2} \end{aligned}\right\} \qquad (5)$$

The correction due to pressure effects [11] leads to the use of

$$\left.\begin{aligned} K_c' &= K_c + K_d \frac{16\lambda^2}{9}(2 - \phi) \\ K_d' &= K_d \end{aligned}\right\} \qquad (6)$$

Note that the true retention coefficient do not only depend on the membrane but also on the rest of the experimental device (cell design, stirrer, etc.) which determines the flux condition on the membrane and control the solute accumulation on the membrane-feed side (making $C_m \neq C_f$). The true retention coefficient, *R*, is higher than the observed one, $R_o = 1 - \left(C_p / C_f\right)$ due to the effect of concentration polarization. Thus, the true retention coefficient needs a careful determination of C_m from the feed concentration, C_f. This can be done by a watchful accounting of the concentration-polarization and mass transfer theory [10] for the feed-membrane interface. Once the true retention has been measured it can be fitted to Equations (4) to (6) to get r_p.

2.4.3 Microscopic examinations

Scanning electron microscopy (SEM) was employed to analyse the structure of prepared membranes with a Quanta 200FEG equipement of FEI. For these studies, membranes were frozen in liquid nitrogen and fractured.

Atomic Force Microscopy (AFM) has been performed with a Nanoscope IIIA. The tapping mode has been used in air, with silicon mono-cantilever probes.

2.4.4 Streaming potential measurements

Electrokinetic properties of the membranes were determined by using streaming potential measurements. These measurements were done by flowing electrolyte solution along the membrane top surface leading to obtain direct data on the electric properties of the membrane skin layer. The streaming potential was measured by using a clamping cell equipped with two $Ag/AgCl_2$ electrodes placed at the module entrance and exit. Two membrane samples were loaded in this holder by facing their skin layers without allowing any permeation through them and creating a channel for the electrolytic solution flow. The experiments were conducted in a 0.001 M KCl solution at 20 ^{o} C. Different streaming potentials were measured for pH values ranging from 3 to 9 using for adjustment 1 M of HCL and NaOH added when needed. The transmembrane pressure varied from 0.1 to 0.9 bar. The Smoluchowski equation was used to correlate streaming potential data with zeta potential.

$$\zeta = \frac{K_m \eta_s}{\varepsilon} \nu_p \qquad (7)$$

ζ is the zeta potential, K_m is the solution conductivity, η_s *is* the solution viscosity, ε *is* the dielectric constant and $\nu_p$is the slope of the streaming potential versus transmembrane pressure. *A d*etailed description of streaming potential theory and measurements can be seen elsewhere [13].

2.4.5 Contact angle measurements

To determine the hydrophobicity properties of the membranes, the contact angle between water and the membrane surface was measured at room temperature using An FTA200 contact angle meter that uses drop shape methods. As the final result, the average of five values of contact angle on different locations of the membranes was used.

The Wenzel model [14] describes the homogeneous wetting regime on a rough surface assuming that the wetting liquid reaches from peaks to valleys on the surface of the wetted surface. This leads to an apparent contact angle (θ_{app}), experimentally obtained, which is related to the actual or Young contact angle (θ_Y), which would be measured if the surface was perfectly smooth and flat. The correlation between both contact angles on a rough surface is given by [15,16]:

$$cos\left(\theta_{app}\right) = r_W \ cos\left(\theta_Y\right) \qquad (8)$$

The r_w is the so called Wenzel's coefficient which is the ratio of the true area of the solid surface to its nominal or projected area (r_w >1). This equation shows, as it is well-known, that when the surface is hydrophobic (θ_Y > 90º), roughness increases hydrophobicity (hinders wettability) because it increases the contact angle. It is also clear that, when the surface is hydrophilic (θ_Y < 90º), roughness increases hydrophilicity (improves wettability) as the contact angle decreases.

2.5 Filtration run and removal experiments

The removal experiments were conducted using synthetic wastewater in a dead–end membrane module equipped with stainless steel cylindrical batch cell (400 cm^3) with magnetic stirring bar covered by PTFE located on magnetic stirrer. The working pressure in the cell, applied by a nitrogen tank, was adjusted at 0.5 – 2 bar. The membrane sheet area was 0.00385 m^2. Deionized water was passed before and after each filtration of wastewater. pH of wastewater was adjusted using 1M HCl and NaOH solutions. The process was operated until the volume of permeate reached 200 mL. In this study we addressed the question of the influence of: SWCNT loading of the membranes, transmembrane pressure, pH of wastewater and the degree of adsorption. The removal effectiveness (E) of both BPA and NP were calculated by:

$$E = \left(1 - \frac{\bar{C}_p}{\bar{C}_f}\right) 100\% \quad (9)$$

$\bar{C}_f$ and $\bar{C}_p$ are the concentrations of micropollutants in the feed reservoir at the beginning of the filtration and in the permeate container at the end of the experiment, respectively. Note that E is similar to $R_o = 1 - \left(C_p / C_f\right)$ but R_o changes with time because it refers to concentrations in the feed and permeate that change with time too. Note that, of course the true retention, $R = 1 - \left(C_p / C_m\right)$, does not change with time although C_m and C_p do.

The degree of adsorption (A) was calculated from recovery ($\tilde{R}$) according to:

$$\tilde{R} = \left(\frac{\bar{C}_r \bar{V}_r + \bar{C}_p \bar{V}_p}{\bar{C}_f \bar{V}_f}\right) 100\% \quad (10)$$

$$A = 100\% - \tilde{R} \quad (11)$$

$\bar{C}_p$, $\bar{C}_r$ are the concentrations of micropollutants in the permeate and retentate respectively and, $\bar{V}_p$, $\bar{V}_r$ are the volume of permeate and retentate at the end of the experiment. $\bar{C}_f$ and $\bar{V}_f$ refer to the feed at the beginning of the experiment.

The concentrations of BPA and NP were determined using solid phase extraction (SPE) and HPLC analysis. For SPE, glass columns filled with C_{18} phase (from Supelco) were used. Before extraction, C_{18} beds were washed with methanol (1mL), acetonitrile (1 mL), deionised water (1mL). 200 mL of sample was drawn through the columns. After the samples had completely passed, SPE bed was dried under vacuum. The extract was eluted with two portions of 1 mL acetonitrile/methanol (60/40, v/v) then eluate was dried under high-purity nitrogen flux. Dried residue was re-dissolved in 1 mL of acetonitrile. The concentration of micropollutants was analysed using high performance liquid chromatography at a wavelength of λ = 220 nm. The chromatograph was equipped with a

chromatography column (Hypersil Gold C18, 5μm particle size, 205mm x 4.6 mm) and an UV-VIS detector. The flow rate of the mobile phase (acetonitrile/deionised water, 85/15, v/v) through the column was 1mL/min. The limit of detection of this method was 0.5 μg/dm^3. The analytical procedure allowed the recovery of compounds from 200 mL of wastewater at the level of 100% and 40% for BPA and NP respectively.

2.6 Study of membrane fouling during micropollutants removal from wastewater

The procedure of fouling analysis was based on the following measurements: deionised water flux (J_w), permeate flux (synthetic wastewater) (J_V), deionised water flux after treatment process (J_{wp}). The fluxes were calculated by Equation (9). The flux recovery (F_R) was calculated as:

$$F_R = \left(\frac{J_{wp}}{J_w}\right) 100\% \tag{12}$$

According to filtration theory, different kinds of resistances occur during the passage of a fluid through a membrane. Permeate flux depends on the membrane resistance and other resistances that are caused by the interaction between feed components and the membrane material and can be calculated by the Darcy law:

$$J_V = \frac{\Delta p}{\eta_p \sum R} \tag{13}$$

η_p is the dynamic viscosity of permeate and $\sum R$ the sum of resistances. The membrane resistance (R_m), the resistance due to irreversible fouling (R_{if}) and the resistance due to reversible fouling (R_{rf}) are described by Equations (14), (15) and (16) respectively.

$$R_m = \frac{\Delta p}{\eta_p J_w} \tag{14}$$

$$R_{if} = \frac{\Delta p}{\eta_p J_{wp}} - R_m \tag{15}$$

$$R_{rf} = \frac{\Delta P}{\eta_p J_V} - R_m - R_{if} \tag{16}$$

The following percentages can be evaluated:

$$r_f = \left(1 - \frac{J_V}{J_w}\right) 100\% = \frac{R_{rf}+R_{if}}{R_{rf}+R_{if}+R_m} 100\% = j_i + j_r \tag{17}$$

$$j_i = \left(\frac{J_w - J_{wp}}{J_w}\right) 100\% = \left(1 - \frac{J_{wp}}{J_w}\right) 100\% = (100 - F_R)\% \quad (18)$$

$$j_r = \left(\frac{J_{wp} - J_V}{J_w}\right) 100\% = \left(F_R + r_f - 100\right)\% \quad (19)$$

r_f is the percentage of fouling resistance per unit of total resistance, j_i is the percentage of loss of flux per unit of initial flux due to irreversible fouling and j_r is the percentage of recovery of flux per unit of initial flux due to the removal of reversible fouling.

3 Results and discussion

The filling of polymer membranes with nanomaterials causes great changes in their structure and properties. Membranes filled with even very small amount of nanotubes have completely different permeation, retention and electrokinetic properties in comparison to a pristine membrane. This can be explained by the fact that the phase inversion runs in a different way. Carbon nanotubes undergo spontaneous aggregation, forming bigger groups [4] that, on one hand, can form voids in membrane structure but, on the other hand, can also block pores, especially if the amount of nanotubes exceeds an optimal concentration [7,17]. Therefore, it is very difficult to unequivocally determine the impact of nanotubes on the membrane. Final properties of a membrane depend on the mutual interaction between nanotubes and polymer within the membrane matrix.

3.1 Effect of SWCNT loading on the membrane water permeability

The mean deionized water flux is shown in Fig. 1 as a function of transmembrane pressure. The water permeation of prepared membranes tended to increase with increasing SWCNT loading within the PES matrix. PES and PES 0.025%SWCNT membranes exhibited very similar fluxes in the whole range of applied pressures. More detailed data are presented in Fig. 2, where water permeability is correlated with the percentage of SWCNT in the loaded membranes.

Fig. 1. Deionized water flux of prepared membranes as function of transmembrane pressure.

Fig. 2. Permeability of the studied membranes as a function of the SWCNT content.

3.2 LLDP

The permeability distributions for the selected membranes are illustrated in Fig. 3.a. It seems clear that data do not fit perfectly to Gaussian distributions. The reason of this is the occurrence of very small pores in the structure of the membranes, that were yet opened even at the highest operational pressure (50 bar),

available in the used setup. In any case not too higher pressures can be used without the risk of distorting membrane structure [18].

However, LLDP measurements, even when working close to the minimum operation range as on this occasion, can supply a lot of important information on membrane structure. Fig. 3.b presents membrane permeability, pore number and area in pores as a function of pore radius, plotted as cumulative curves.

Most of the pores (90%) were at the level of 6-8 nm, depending on the membrane modification content, with slight differences between them. As commented in section 3.1, an increase in the SWCNT content leads to a membrane with a higher permeability. This has also been observed in the LLDP results. Consequently, membranes with higher porosities and or smaller equivalent thicknesses were formed and the permeability increased when the proportion of nanotubes augmented.

Moreover, using the calculation procedure described by Calvo et al. [9], the molecular weight cut off was estimated. This method is based on finding the pore size that constitutes 90% of the total population of pores in the membrane. It was done, as shown in Fig 3 b by interception of the dotted lines plotted on graphs. The estimated MWCO is depicted in Table 4. MWCO estimated was around 80 KDa for all samples, with a slight tendency to increase as the content of Carbon Nanotubes increase. For this estimation it is assumed that dextran acquires a prolate ellipsoidal shape in solution showing a relative rigidity without any interaction to each other and with the membrane material [19], then allowing penetration only of molecules smaller than pores, excluding the possibility of penetration via another mechanism.

Fig. 3. Porous properties of selected membranes: (a,b,c) permeability distribution, (d,e,f) - cumulative values of permeability, pore number and pore area.

Table 3 Morphological parameters and MWCO for selected membranes from LLDP.

3.3 Pore Sizes by Retention Tests

The mean pore sizes as obtained from retention tests are shown in Fig. 4 along with those obtained from LLDP. It seems clear that these results support each other and clearly show that there is not a correlation of pore size with the amount of SWCNT contained in the membranes studied.

Fig. 4. Average pore radii obtained from retention tests and LLDP versus the percentage of SWCNT loading. The solid line corresponds to the linear fitting of retention tests results.

In Fig. 5, the corresponding true retention coefficients are plotted along with the permeability measured during the retention tests with the Dextrane solutions. Note that permeability in Fig. 5 compares well with, but is smaller than, that (for pure water) shown in Fig. 2.

Fig. 5. True retention and permeability during retention tests as a function of the percentage of SWCNT loading.

According to Figs. 4 and 5, It is obvious that, in effect, neither pure water permeability nor the volume flow during retention tests are clearly correlated with pore radii. Note that retention tests give an approximate average retention of 75 % for a dextrane of 40 KDa that is not far from the molecular weight cut off of 80 KDa predicted by LLDP.

3.4 Microscopic characterization of PES/nanocomposite membranes

In order to reveal the impact of SWCNT loading to PES membranes on their final morphology and structure, SEM analysis for membranes without nanotubes (PES) and with the lowest (PES 0.025%SWCNT) and the highest amount of nanotubes (PES 0.5%SWCNT) was performed.

The skin surface of pristine PES membrane looked dense and closed at the magnification of our images, which indicates a lack of big-size pores while the compactness of the surface of the nanocomposite membranes was rather lower (Fig. 6 a). The surface of PES 0.025%SWCNT looks a little coarser in Fig. 6 b. Moreover, in case of PES 0.5%SWCNT, the SEM micrographs present very loose cross-linked surface (Fig. 6 c and 6 d). Similar observations were commented by Shen et al. [20] that observed a crosslinking area on the top surface of nanocomposite membranes and interpreted it as a consequence of the connection of nodules in polyamide membranes. This phenomenon was also reported by Wu et al. [21] that pointed out that the clustering of nanotubes during phase inversion was the cause of very large densities of nanotubes within the membrane matrix because the steric hindrance and electrostatic interactions between nanotubes and polymer chains were not enough to prevent aggregation. Thus, spontaneous and preferential aggregation of nanotubes would lead to the formation of grains on the surface of membrane and create a cross-linked top layer with big voids. Computerized image analysis of such voids gives a mean radius of 0.1 μm broadly distributed with some voids until 0.25 μm in radius. However, these surface cavities could remain closed to flow, in view of the modest increase of permeability for PES 0.5% SWCNT.

Fig. 6. SEM images of top surface of prepared membranes: (a) PES, (b) PES 0.025%SWCNT, (c, d) different magnifications of PES 0.5%SWCNT.

All membranes had asymmetric structure consisting of a porous support and a thinner top layer (Fig. 7). Typically the cross section of polyethersulfone membranes reveals a sponge like structure. In our case, the size of the voids on the top layer increased with increasing SWCNT loading. This is particularly evident when cross sections of PES and PES 0.5% SWCNT membranes were compared as demonstrated in Figs. 7 b and 7 f. The structure of the top layer of PES 0.5% SWCNT exhibited clear void spaces as can be confirmed in Fig. 7 g. Of course, microscopy cannot confirm or reject that they could cross the membrane to constitute real pores.

The sub-layers differed greatly in prepared membranes. In particular, the number of macrovoids was considerably lower in membranes without nanotubes in comparison to membranes with a higher amount of nanotubes that presented bigger and more abundant voids leaving thinner inter-void walls. This would imply both higher porosities and lower equivalent membrane thickness for the SWCNT loaded membranes.

The differences in the structure of loaded and unloaded membranes could be due to the previously mentioned action of the high concentration of nanotubes within the PES matrix that could lead to a partial blocking of pores by clustered aggregations of nanotubes. On the other hand a similar effect was demonstrated by Celik et al. and Shahid et al. [2,22] who explained it by an increase of viscosity in the PES-SWCNT casting solution, that caused slower run of phase inversion consequently leading to the formation of less macrovoids in the sub-layer and pores with bigger sizes within all the membrane structure. Due to the very small size and diameter of the nanotubes, it was impossible to distinguish the nanotubes and their dispersion in the cross sectional view of PES-SWCNT matrix attending to the limitations of SEM.

Fig. 7. SEM cross sectional images (different magnifications) of prepared membranes: (a, b) PES, (c, d) PES 0.025%SWCNT and (e,f,g) different magnifications of PES 0.5%SWCNT.

Complementary information on the impact of nanotubes on the topography of PES-SWCNT membranes was obtained by means of AFM analysis. The images presented in Fig. 8 are in good correspondence with SEM images i.e. similar trends for the changes in the surface topography were observed. The surface of pristine PES membrane (Fig. 8.a) is more compact, at the magnification used, than that of nanocomposite membranes (Fig. 8.b). The surface of PES 0.1%SWCNT is more nodular (Fig 8 b). Note that bright areas indicate the heights on the membrane surface, while the dark zones correspond to valleys. As illustrated in Table 5 the average roughness, R_q, of membranes, as measured in 1μmx1μm pictures, was not greatly affected by nanotubes for membranes with lower SWCNT loading, however changed greatly by adding 0.5%SWCNT. The average roughness of the pristine PES slightly decreased from 4.35 nm to 3.83 . nm for PES 0.1%SWCNT. In low SWCNT loading, because of weak intermolecular interactions between SWCNT, the nanotubes would be more regularly distributed within the membrane structure and the surface should become smoother. For PES 0.5%SWCNT the SWCNT density is high enough to contribute to the formation of bigger agglomerates of nanotubes inducing an increase in the size of voids and in the surface roughness.

Fig. 8. AFM images of the surface of membranes: a - PES, b - PES 0.1%SWCNT. The size of the scanned areas is 1μmx1μm.

Table4. Average roughness of membranes measured in 1μmx1μm pictures.

3.5 Effect of pH on zeta potential of PES/nano-composite membranes

The apparent zeta potential versus pH is presented in Fig. 9. From these results, a few deductions can be made regarding the SWCNT loaded membranes. Firstly, prepared membranes were positively charged at low pH with an isoelectric point between 4 and 7 and negatively charged at high pH. Negative charge under alkaline conditions is obvious for membranes made of polyethersulfone, due to the chemical characteristics of sulfonic group that dissociates notably at high pH. Positive charge of PES membranes can be a consequence of adsorption of positive ions during streaming potential measurements. The cation effect influencing the zeta potential of PES membranes was confirmed in several studies [23,24,25]. Secondly, prepared membranes with increasing SWCNT content acquired more negative charge from lower pH with the subsequent lessening of the isoelectric point. This agrees with the known negative charge of carbon surfaces with isoelectric points around 2.5 [26]. In our case the charge would be even more negative because the nanotubes are recovered with carboxyl groups. This enhancement in zeta potential, due to the addition of nanotubes to the polymer matrix was also observed by Shen et al. [20].

Fig. 9. Calculated zeta potential of the prepared membranes.

3.6 Hydrophobic/hydrophilic properties of PES/nanocomposite membranes

Hydrophobic/hydrophilic properties of the membranes depend primarily on the membrane polymer. Obviously, the addition of nanotubes changes these properties. Generally, carbon nanotubes are hydrophobic (without additional chemical functionalization or acid treatment) and their addition to polymer increase hydrophobicity [27,28]. Whereas, incorporation of even small amounts of functionalized nanotubes can raise the hydrophilicity of the polymer matrix [1,21,29].

As seen in Fig. 10, the calculated Young contact angle (from AFM analysis, using Equation (10)) was in all cases very similar to apparent contact angle. Moreover, the apparent contact angle of the membranes decreased from 69.4^{o} to 62.5^{o} when the SWCNT loading increased from 0 to 0.05%, which corresponds to a very small increase of hydrophilicity. However, the hydrophilicity decreased, also very slightly, when the nanotubes loading was in the range 0.1 - 0.5 %. Which is not surprising when one considers that carbon surfaces are considered to have contact angles around 90^{o} [30] but are added in very small amounts. A similar trend was observed in several studies [31,32] and interpreted there as caused by an irregular collocation of nanoparticles in the membrane structure leading to a slight decrease of water permeation due to a decrease of hydrophilicity. In any case it is interesting to point out that the changes in hydrophilicity are quite small.

Fig. 10. Apparent and Young contact angle of prepared membranes as a function of SWCNT loading.

In summary, the SWCNT loading in the polymer matrix induces two major effects on the membrane properties. A very evident one is a change in the membrane structure that could lead to higher porosities or lower thicknesses, as mentioned above, without quite significant changes in pore sizes, and the other, strongly depending on chemical functionalization of nanotubes, is the increase of hydrophobicity of the membranes. Both factors have been confirmed here and could influence permeation of the membranes. In fact, the surface and top layer of PES 0.5%SWCNT was looser and with higher apparent porosity than pristine membrane (Figs. 6 and 7), consequently it could lead to a high permeability. Nevertheless it is worth mentioning that it is the actual porosity of the active layer which determines permeability rather that the easily observable porosity of the membrane sublayers. The morphology of PES 0.025% was not significantly affected by SWCNT due to very small SWCNT loading (Fig. 7 a-d). The slight increase of water permeation could be a consequence of a balance of the minor decrease of hydrophilicity (that would lead to somewhat lower permeabilities) and of the increase of porosity (or decrease of the effective thickness) of the selective layer (active layer) of the membranes with increasing SWCNT content.

3.7 Removal of micropollutants

3.7.1 Effect of SWCNT loading

Fig. 11 illustrates the effectiveness of the removal of micropollutants and the permeate flux for different loadings of carbon nanotubes. It is obvious that the amount of nanotubes had an important role on treatment effects due to changes in membrane structure and properties. The increase of SWCNT loading caused a consistent increase in the effectiveness of micropollutants removal. Membrane PES 0.5%SWCNT was an exception showing a reduction of the micropollutants retention to a level similar to the pristine PES membrane. This effect is difficult to explain. On one hand, a high amount of nanotubes in the membrane should enhance sorption due to the increase of sorption sites in PES-SWCNT matrix. On the other hand the structure of PES 0.5%SWCNT is evidently more opened with less surface for adsorption of the micropollutants. In this case, the higher porosity would lead to higher fluxes that could disturb and hold back micropolutant adsorption and retention.

Anyway, it seems clear that filling of PES membranes with SWCNT is favourable only up to a relatively low amount of nanotubes in polymer matrix. Similar observation were demonstrated by Vatanpour et. al. [1] that showed that an optimal effect in the rejection capability of nanocomposite PES membranes was observed for a low quantity of nanotubes. Ghaemi et al. observed the enhancement of the retention of nitrophenols when increasing the concentration of nanoparticles (only within a certain range) in polyethersulfone membranes. They correlated this effect with obstructive properties due to the formation of a layer of nanoparticles

on the membrane surface which successfully limited the diffusion of nitrophenols adsorbed inside nanocomposite membranes [7].

We also found that the removal of nonylphenol was higher than for bisphenol A. Higher removal efficiency of nonylphenol can be considered as an effect of higher hydrophobicity of this compound, resulted in an easy and favourable retention on nanocomposite membranes. The octanol-water partition coefficient ($\log K_{ow}$) describes the affinity of compounds to sorption. When the value of $\log K_{ow}$ is lower than 2, the compound is hydrophilic, and higher $\log K_{ow}$ means that the substance is more hydrophobic and will show more affinity to sorption and aggregation. As seen in Table 2 the value of $\log K_{ow}$, for NP is twice that for BPA.

In several studies, sorption of organic micropollutants on membrane surfaces is considered as one of the main mechanisms influencing retention [33,34]. It is also recognized as a reason of unexpected high retention in ultrafiltration, where significant sieving effects were excluded [35]. In order to reveal the influence of adsorption of micropollutants on retention, the degree of adsorption of BPA and NP on the surface for PES and PES 0.1%SWCNT membranes was determined (Fig.12). This revealed that, in effect, the removal of micropollutants was accompanied by their adsorption on the membrane; moreover, that removal is only slightly higher than adsorption. Of course adsorption must be the most relevant factor explaining BPA and NP retention attenfing to their small size. In the case of PES, the degree of adsorption was at the level of 35% and 45% for BPA and NP respectively. A significantly higher value of the parameter reached 56% and 76% was obtained for PES 0.1%SWCNT. The results confirm the key role of nanotubes in the increase of sorption of certain micropollutants during filtration that leads to enhance retention.

Fig. 11. Effect of SWCNT loading on wastewater permeability (at 0.5 bar) and on removal of micropollutants.

Fig. 12. Effectivenes of removal and adsorption of micropollutants: (a) BPA, (b) NP for selected membranes.

3.7.2 Effect of the applied transmembrane pressure

As seen in Fig. 13, an increase of pressure caused a reduction of the removal of BPA for PES and PES 0.1%SWCNT membranes. A higher operational transmembrane pressure would increase convection and would also lead to a faster passage of the solution through the membranes reducing the retention coefficient. The sorption potential of nanotubes mainly stems from large specific surface areas, hydrophobic (π-π) or electrostatic interactions with very fast adsorption rates, guarantying the use of their total sorption capacity in a quite short times [4,36]. In any case, for the membranes filled with nanotubes, the rate of passage determines the contact time between sorbent and pollutants in solute. Therefore, when the value of pressure was low, contact time was high and nanotubes can adsorb micropollutants more effectively.

Fig. 13. Effect of transmembrane pressure on the effectiveness of removal of bisphenol A.

3.7.3 Effect of pH

The pH of the feed solution is an important factor affecting the retention process because of its influence on the stability and chemical form of some organic pollutants and also on the zeta potential of the membranes. This effect is shown for BPA in Fig. 14 and the membranes: PES, PES 0.025%SWCNT and PES 0.1%SWCNT. The retention was at similar levels between pH 3 and 7 for PES and PES 0.025%SWCNT membranes. In the case of PES 0.1%SWCNT, a slight increase in removal was observed when the feed pH exceeded 7. However, in all cases, a really noticeable increase of BPA removal was observed when the solution pH reached 9. As mentioned above, a change of pH can influence retention in two ways. Firstly, BPA is a weak acid with a pKa value of 9.6–10.2. Therefore in alkaline solution, BPA molecules dispose a proton and transform into bisphenolate anions. Secondly, in alkaline conditions, the surfaces of the membranes are more negatively charged due to significant dissociation of sulfonic and carboxyl groups (Fig. 9). Thus, an increase of removal when pH>pKa can be consider as an effect of growing repulsion forces between bisphenolate anions and the negatively charged membrane surface.

It seems clear that, at all pH, removal is better for high enough contents of SWCNT within the PES matrix. PES0.1%SWCNT has 4 times nanotube content than the PES0.025%SWCNT membrane.

Fig. 14. Effect of the wastewater pH on the effectiveness of removal of BPA.

3.8 Membrane fouling during wastewater treatment

The membrane fouling, typically disturbing pressure driven membrane processes, is a consequence of the deposition of some feed components on the membrane surface or inside the membrane pores leading to a more or less fast flux decline. Intensity of fouling depends on: the chemical composition of feed (concentration of pollutants), pH of feed, operational parameters (feed velocity, pressure and temperature) and also on the properties of membrane materials and their interaction with the solute and solvent. Fig. 15 shows flux decline during deionised water and wastewater filtration for selected membranes. Firstly, these results clearly indicate that PES-SWCNT membranes exhibited higher flux than pristine PES, as already pointed out. Secondly, the highest difference between the deionised water flux and the wastewater permeate flux in the first 60 minutes appeared for the PES membrane. On the contrary, permeate flux obtained for

nanocomposite membranes was more similar to the flux of deionised water. In other words, PES membranes were more sensible to fouling than the PES-SWCNT ones. Moreover, for nanocomposite membranes, the obtained flux recovery was a little higher in comparison to pristine PES (Table 6). This could be attributed to the relatively hydrophobous character of both the solute and the loaded membrane.

The major types of membrane resistances were calculated and depicted in Table 6. Among the considered resistances, the most significant one was the membrane resistance. The highest membrane resistance was observed for the pristine PES, and the lowest for PES 0.1%SWCNT. According to data from SEM examination (Fig.1 and 2), the structure of nanocomposite membranes was more porous than that of the pristine PES. Thus, higher porosities (and/or smalles equivalent thicknesses) of PES-SWCNT membranes exhibited lower membrane resistances than those of PES membranes. This leads to higher permeabilities (Figs. 8 and 9). It is also clear, that the cake formation and fouling resistances of pristine PES were high compared to these of PES-SWCNT membranes.

Fig.15. Different fluxes during filtration: Deionised water flux for pure membranes (0-60 min), wastewater flux (70-120 min) and deionised water flux after wastewater treatment (130-190 min).

Table5. Different kinds of resistances and flux recovery for prepared membranes.

The participation of reversible and irreversible fouling in total fouling is illustrated in Fig. 16. The first one can be easily removed and the permeability of membranes is restored. Whereas irreversible fouling is caused by permanent adsorption of pollutants especially into membranes pores. In this case, initial hydraulic permeability cannot be restored, even using chemical cleaning [37]. Generally, for all membranes, reversible fouling was higher than the irreversible one. Reversible and irreversible fouling of PES 0.025%SWCNT and PES 0.1%SWCNT membranes were roughly at the same level. However, pristine PES membranes exhibited significantly higher reversible and slightly higher irreversible fouling in comparison to PES-SWCNT. The main reason can be that the negative charge of the pristine PES membrane is lower than those of the nanocomposite membranes at pH of 7 (Fig. 9). In fact, the membrane surface of PES membranes could be even uncharged at nearly neutral conditions. Thus, substances included in synthetic wastewater (i.e. organic micropollutants, salts and proteins, carbohydrates, vitamins, fats included in peptone and bouillon), described in section 2.2, could easily deposit on the membrane surface. This effect can also be due to the higher hydrophobicity of PES in comparison to PES 0.025%SWCNT (Fig. 5). Furthermore some authors suggest that fouling is more intensive on the more rougher valley-surface due to preferential adsorption of pollutants on the valleys [1,38]. Among the two studied nanocomposite membranes, slightly higher total fouling was observed for PES 0.1%SWCNT that can be explained by the higher hydrophobicity of this membrane.

Fig. 16. Magnitude of the percentages defined in Equations (19) – (21) for some membranes.

4 Conclusions

It has been shown that the addition of SWCNT nanotubes improves effectiveness of removal and adsorption of estrogenic micropollutants as tested with Bisphenol-A (BPA) or 4,4'-(propane-2,2-diyl)diphenol and 4-Nonylphenol (NP) (4-(2,4-dimethylheptan-3-yl)phenol). Increasing the SWCNT content increases removal and reduces fouling both reversible and irreversible. The same tendency to increase micropolutants removal is found when pH is set to alkaline.

An increase in the transmembrane applied pressure decreases removal more steeply for the membranes containing more SWCNT. Actually most of the removal efficiency is attributable to the adsorption of micropollutants that increases with the SWCNT content.

No clear influence of the SWCNT content on pore sizes has been detected. Although the structure of the more porous layers of the membranes changes to include less but bigger voids suggesting a similar increase in porosity with a parallel decrease of the equivalent thickness of the active layer; this cannot be proved by the microscopic techniques used here but is clearly suggested by the LLDP, retention and pure water permeability results.

The isoelectric point of the SWCNT containing membranes decreases when the content of nanotubes increases. The membranes are thus more negatively charged within wider pH ranges. The membranes are also less hydrophilic when loaded with increasing amounts of nanotubes. Given that BPA and NP are hydrophobous, this explains the high adsorption leading to the detected increase of removal for increasing SWCNT contents.

Too high SWCNT contents lead to a saturation of removal probably because high porosities lead to a decrease in adsorption due to both a decrease in the available surface and a sweeping action of convection through the membrane.

5 Acknowledgements

This work was performed with financial support from the National Science Center Poland under grant “The conception of removal of chosen micropollutants with estrogenic biological activity from biologically treated effluents using integrated system comprised of sorption and pressure-driven membrane techniques” - No. DEC-2011/01/n/st8/02413. The authors would like to thank BASF Company for providing polyethersulfone. Spanish authors would like to thank the Spanish MINECo projects MAT2011-25513 and CTQ2012-31076 and to the Junta de Castilla y León through the project VA248U13.

[1] V. Vatanpour, S. Madaeni, R. Moradian, S. Zinadini, B. Astinchap, Fabrication and characterization of novel antifouling nanofiltration membrane prepared from oxidized multiwalled carbon nanotube/polyethersulfone nanocomposite, J. Membr. Sci. 375 (2011) 284-294.

[2] M. Shahid, D. Fierro, K. Buhr, J. Wind, B. Du, A. Boschetti-de-Fierro, V. Abetz, Multi-walled carbon nanotubes (MWCNTs) mixed polyacrylonitrile (PAN) ultrafiltration membranes, J. Membr. Sci. 403-403 (2012) 101-109.

[3] X. Qu, P. Alvarez, Q. Li, Applications of nanotechnology in water and wastewater treatment, Water Res. 47 (2013) 3931-3946.

[4] J. Bohdziewicz, G. Kamińska, Kinetics and equilibrium of the sorption of bisphenol A by carbon nanotubes from wastewater, Water Sci. Technol., 68 (2013) 1306-1314.

[5] P. Daraei, S. Madaeni, N. Ghaemi M., Khadivi, B. Astinchap, R. Moradian, Enhancing antifouling capability of PES membrane via mixing with various types of polimer modified Multi-walled carbon nanotube, J. Membr. Sci. 444 (2013) 184-191.

[6] V. Vatanpour, S. Madaeni, L. Rajabi, S. Zinadini, A. Derekhshan, Boehmite nanopartilces as a new nanofiller for preparation of anifouling mixed matrix membranes, J. Membr. Sci. 401-401 (2012) 132-143.

[7] N. Ghaemi, S Madaeni, A. Alizadeh, H. Rajabi, P. Daraei, Preparation and characterization and performance of polyethersulfone/organically modified montmorillonite nanocomposite membranes in removal of pesticides, J. Membr. Sci. 382 (2011) 135-147.

[8] J. Calvo, A Bottino, G. Capannelli, A. Hernandez, Comparison of liquid-liquid displacement porosimetry and scanning microscopy image analysis to characterise ultrafiltration track-etched membranes, J. Membr. Sci. 239 (2004) 189-197.

[9] J. Calvo, R. Peinador, P. Pradanos, L. Palacio, A. Bottino, G. Capannelli, A. Hernandez, Liquid-liquid displacement porometry to estimate the molecular weight cut-off of ultrafiltration membranes, Desalination 268 (2011) 174-181.

[10] N. García-Martín, V. Silva, F.J. Carmona, L. Palacio, A. Hernández, P. Prádanos, Pore size analysis from retention of neutral solutes through nanofiltration membranes. The contribution of concentration–polarization, Desalination 344 (2014) 1–11.

[11] V. Silva, P. Prádanos, L. Palacio, A. Hernández, Alternative pore hindrance factors: What one should be used for nanofiltration modelization?, Desalination 245 (1-3) (2009) 606-613.

[12] Dechadilok, P., W. M. Deen , Hindrance Factors for Diffusion and Convection in Pores, Ind. Eng. Chem. Res. 45 (21) (2006) 6953-6959.

[13] F. Martinez, A. Martin, J. Malfeito, L Palacio, P. Prádanos, F. Tejerina, A. Hernández, Streaming potential through and on ultrafiltration membranes. Influence of salt retention, J. Membr. Sci. 206 (2002) 431-441.

[14] R.N. Wenzel, Surface roughness and contact angle, J. Phys. and Colloid Chem. 53 (1949) 1466-1467.

[15] A. Marmur, Wetting on hydrophobic rough surfaces: to be heterogeneous or not to be?, Langmuir 19 (2003) 8343-8348.

[16] A. Marmur, Penetration and displacement in capillary systems, in: M. Schrader, G. Loeb (Eds.), Modern Approaches to Wettability, Springer US, 1992, pp. 327-358.

[17] B.-H. Jeong, E.M.V. Hoek, Y. Yan, A. Subramani, X. Huang, G. Hurwitz, A.K. Ghosh, A. Jawor, Interfacial polymerization of thin film nanocomposites: A new concept for reverse osmosis membranes, J. Membrane Sci. 294 (2007) 1-7.

[18] J.I. Calvo, A. Bottino, G. Capannelli, A. Hernández, Pore Size Distribution of Ceramic UF Membranes by Liquid-liquid Displacement Porosimetry, J. Membrane Sci. 310 (2008) 531-538.

[19] M.P. Bohrer, W. M. Deen, C. R. Robertson, J. L. Troy, B. M. Brenner, Influence of molecular configuration On the passage of macromolecules across the glomerular capillary wall, J. Gen. Physiol. 74 (1979) 583-593.

[20] J. Shen, C. Yu, H. Ruan, C. Gao, B. Van der Bruggen, Preparation and characterization of thin nanocomposite membranes embedded with poly(methyl methacrylate) hydrophobic modified multiwalled carbon nanotubes by interfacial polymerization, J. Membr. Sci. 442 (2013) 18-26.

[21] H. Wu, B. Tang, P. Wu, Novel ultrafiltration membranes prepared from a multi-walled carbon nanotubes polymer composite, J. Membr. Sci. 362 (2010) 374-383.

[22] E. Celik, H. Park, H. Choi, H. Choi, Carbon nanotube blended polyethersulphone membranes for fouling control in water treatment, Water Res. 45 (2011) 274-282.

[23] N. Lawrence, J. Perera, M. Iyer, M. Hickey, G. Stevens, The use of streaming potential measurements to study the fouling and cleaning of ultrafiltration membranes, Sep. Purif. Technol. 48 (2006) 106-112

[24] S. Salgin, U. Salgin, N. Soyer, Streaming potential measurements of polyethersulfone ultrafiltration membranes to determine salt effects on membrane zeta potential, Int. J. Electrochem. Sc., 8, (2013) 7073-7084.

[25] M. Nystrom, M. Lindstrom, E. Matthiasson, Streaming potential as a tool in the characterization of ultrafiltration membranes, Colloids Surface 36 (1989) 297–312.

[26] G.I. Titelman, V. Gelman, S. Bron, R.L. Khalfm, Y. Cohen and H. Bianco-Peled, Characteristics and microstructure of aqueous colloidal dispersions of graphite. Carbon 43 (2005) 641-649.

[27] J. Lee, S. Lee, D. Kimb, Y. Park, The structural and surface properties of carbon nanotube synthesized by microwave plasma chemical vapor deposition method for superhydrophobic coating, Thin Solid Films, 546 (2013) 94-97.

[28] M. Clark, R. Krishnamoorti, Near-superhydrophobic behaviour of multi-walled carbon nanotube thin films, Thin Solid Films, 520 (2012) 4332-4338.

[29] R. Saranya, G. Arthanareeswaran, D. Dionysiou, Treatment of paper mill effluent using Polyethersulfone/functionalized multiwalled carbon

nanotubes based nanocomposite membranes, Chem. Eng. J., 236, (2014), 369-377.

[30] Z. Li, Y.Wang, A. Kozbial, G. Shenoy, F. Zhou, R. McGinley, P. Ireland, B. Morganstein, A. Kunkel, S. P. Surwade, L. Li, H. Liu, Effect of airborne contaminants on the wettability of supported graphene and graphite, Nat. Mater., 12 (2013) 925–931.

[31] Y. Yang, P. Vang, Preparation and characterizations of a new PS/TiO_2 hybrid membranes by sol-gel process, Polymer, 47, (2006), 2683-2688.

[32] S. Qui, L. Wu, X. Pan, L. Zhang, H. Chen, C. Gao, Preparation and properties of functionalized carbon nanotubes/PSF blend ultrafiltration membranes, J. Membr. Sci. 342 (2009) 165-172.

[33] A. Schäfer, I. Akanyeti, A. Semião, Micropollutant sorption to membrane polymers: A review of mechanisms for estrogens, Adv. Colloid Interfac., 164 (2011) 100-117.

[34] M. Dudziak, Retention of mycoestrogens in nanofiltration. Impact of feed water chemistry, membrane properties and operating process conditions, Environ. Prot. Eng., 38 (2012) 5-17.

[35] Y. Yoon, P. Westerhoff, S. A. Snyder, E. C. Wert, J. Yoon, Removal of endocrine disrupting compounds and pharmaceuticals by nanofiltration and ultrafiltration membranes, Desalination, 202 (2007) 16-23.

[36] Q. Liao, J. Sum, L. Gao, The adsorption of rescorcinol from water using multi-walled carbon nanotubes, Colloid. Surface., 312 (2008) 160-165.

[37] W.S. Winston Ho, K. K. Sirkar, Membrane handbook, Springer, New York, 1992.

[38] D. Rana, T. Matsuura, Surface modifications for antifouling membranes, Chem. Rev. 110 (2010) 2448-2471.

Figure

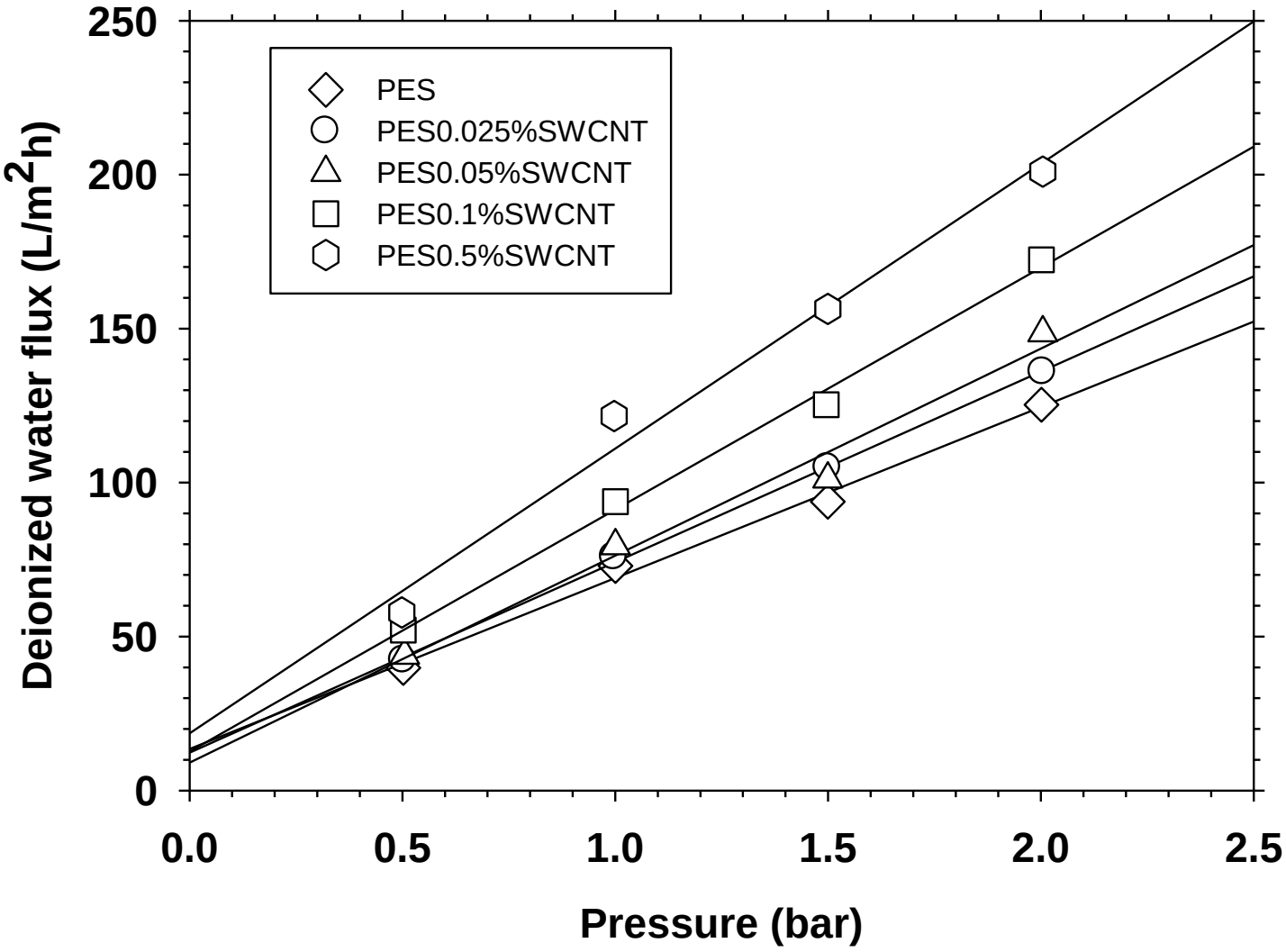

Fig. 1. Deionized water flux of prepared membranes as function of transmembrane pressure.

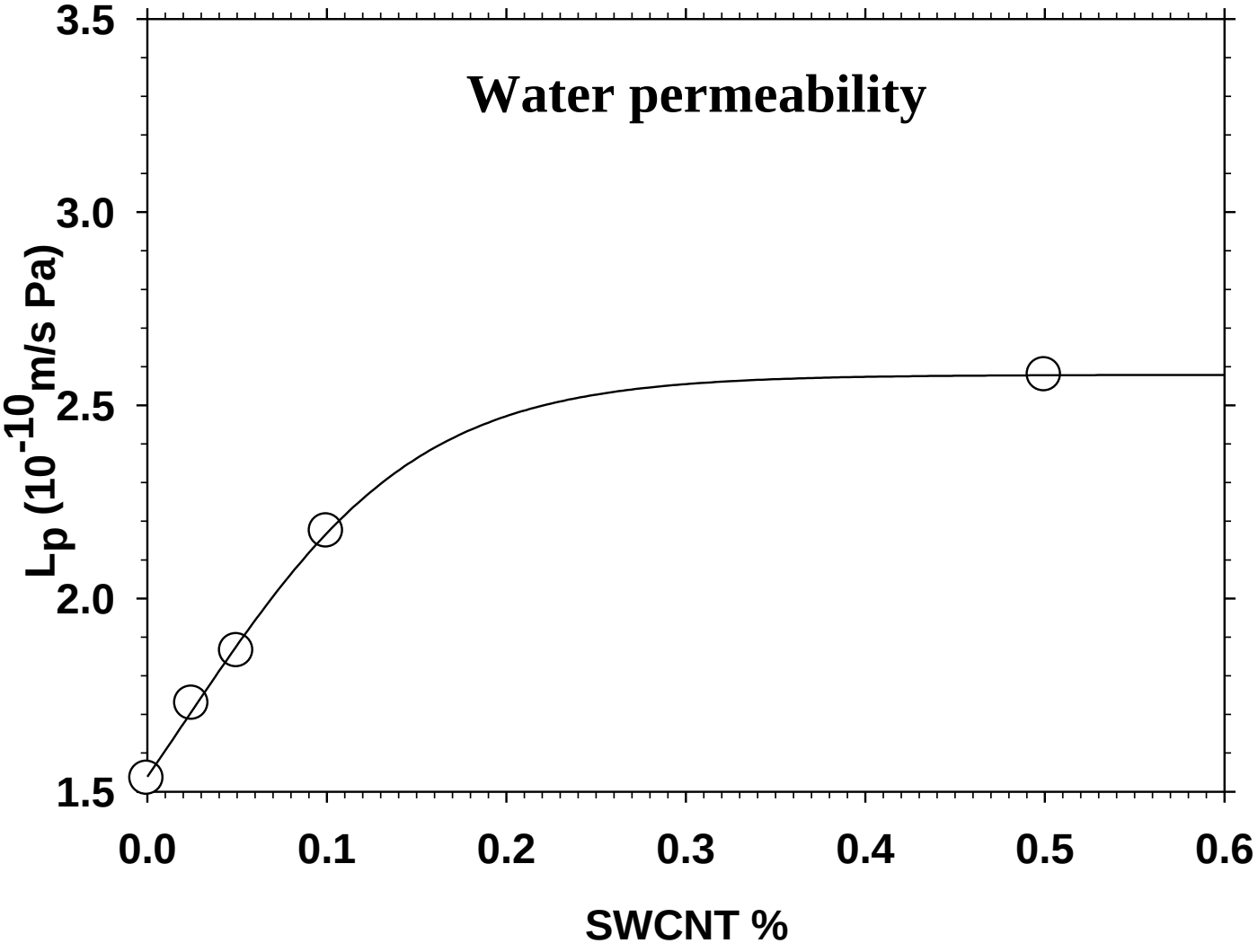

Fig. 2. Permeability of the studied membranes as a function of the SWCNT content.

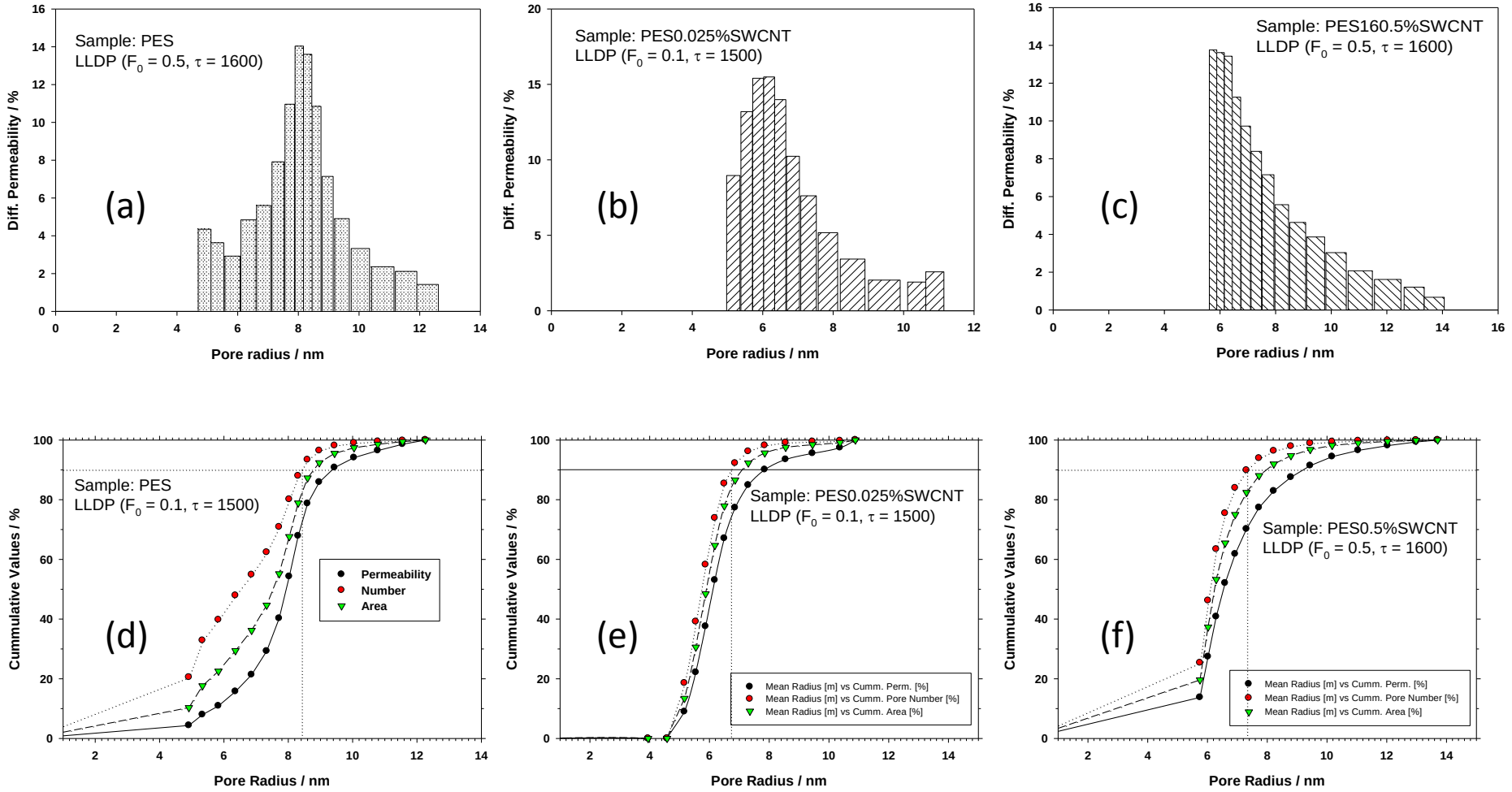

Fig. 3. Porous properties of selected membranes: (a,b,c) permeability distribution, (d,e,f) - cumulative values of permeability, pore number and pore area.

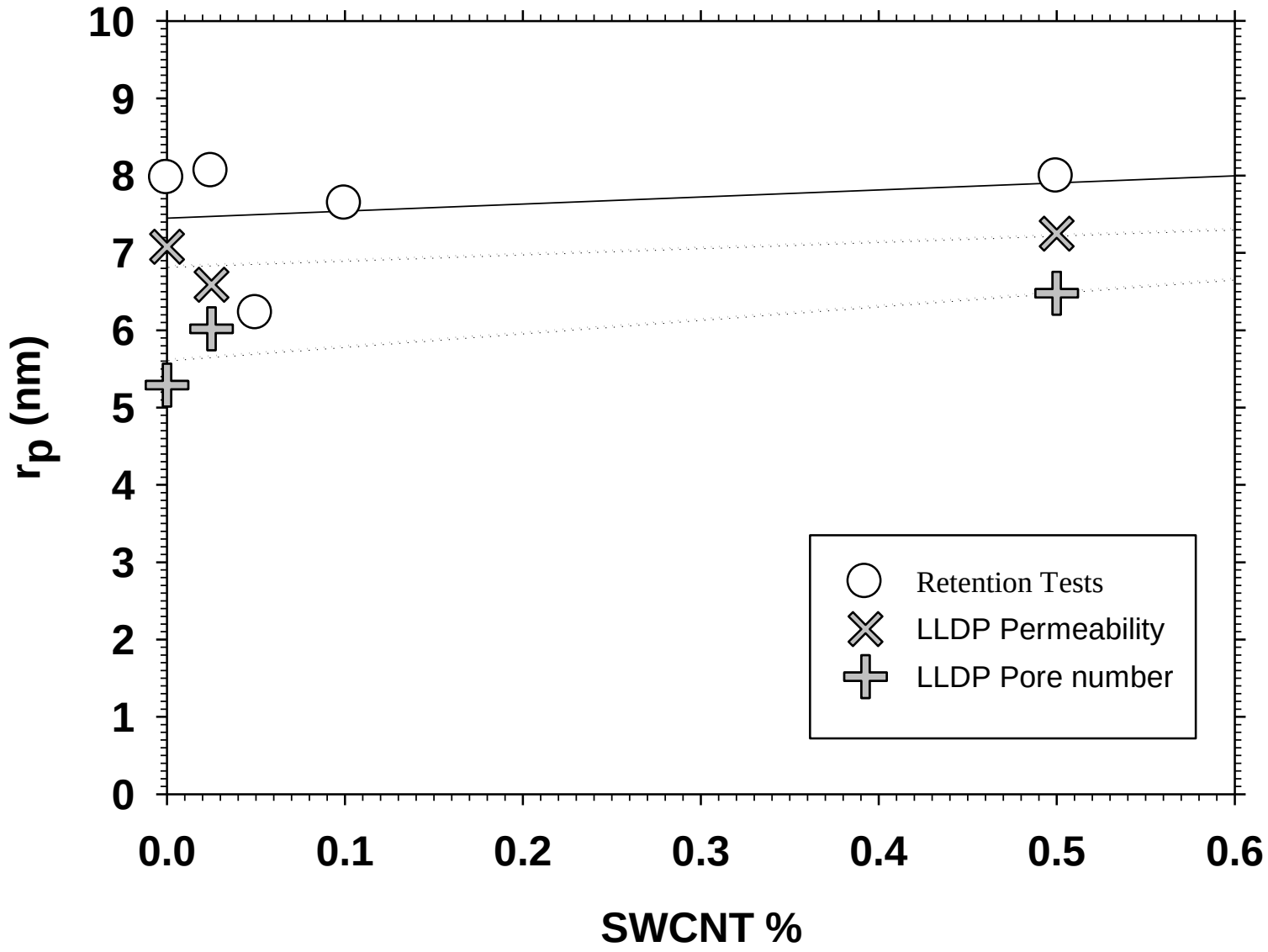

Fig. 4. Average pore radii obtained from retention tests and LLDP versus the percentage of SWCNT loading. The solid line corresponds to the linear fitting of retention tests results.

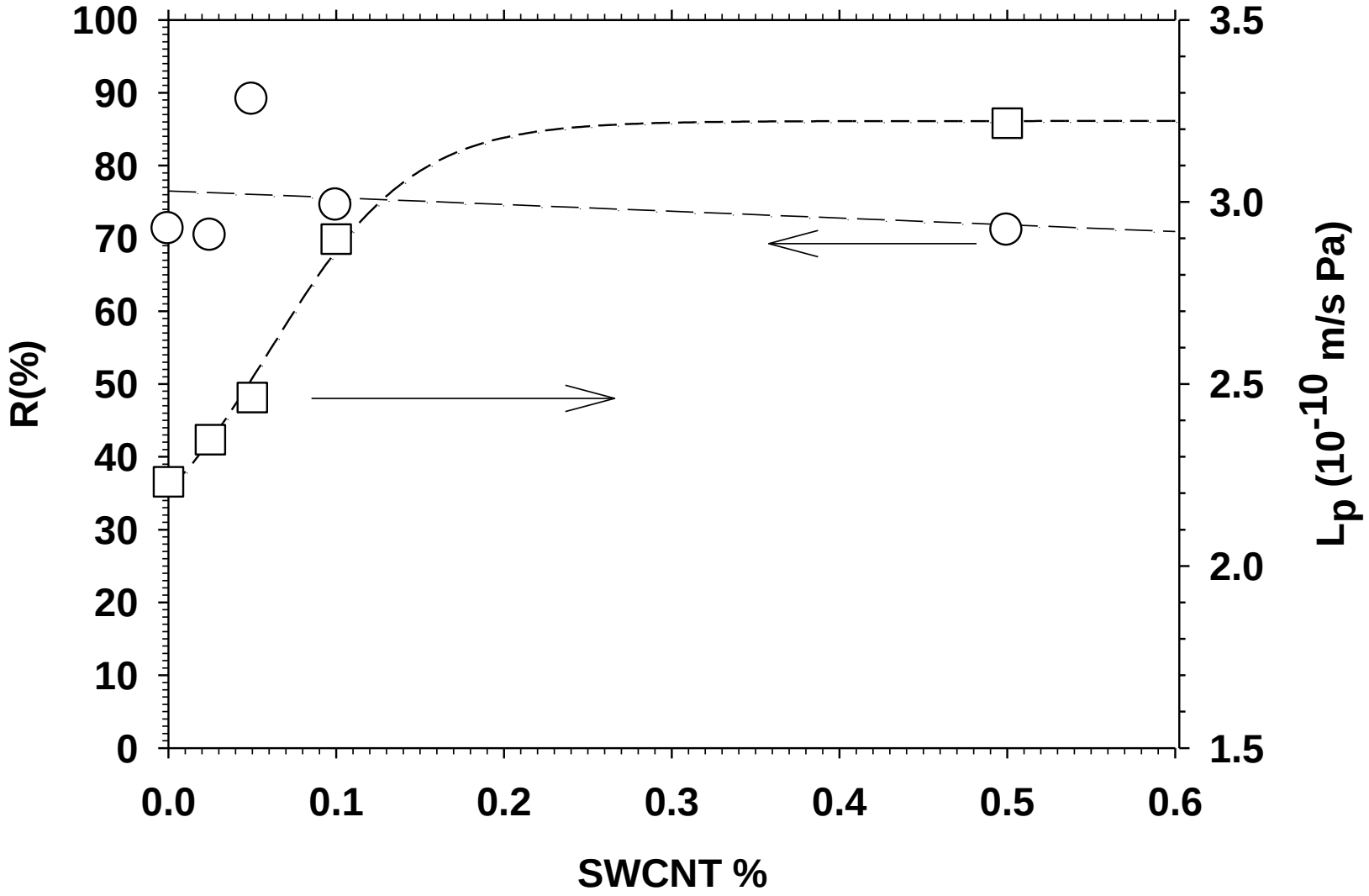

Fig. 5. True retention and permeability during retention tests as a function of the percentage of SWCNT loading.

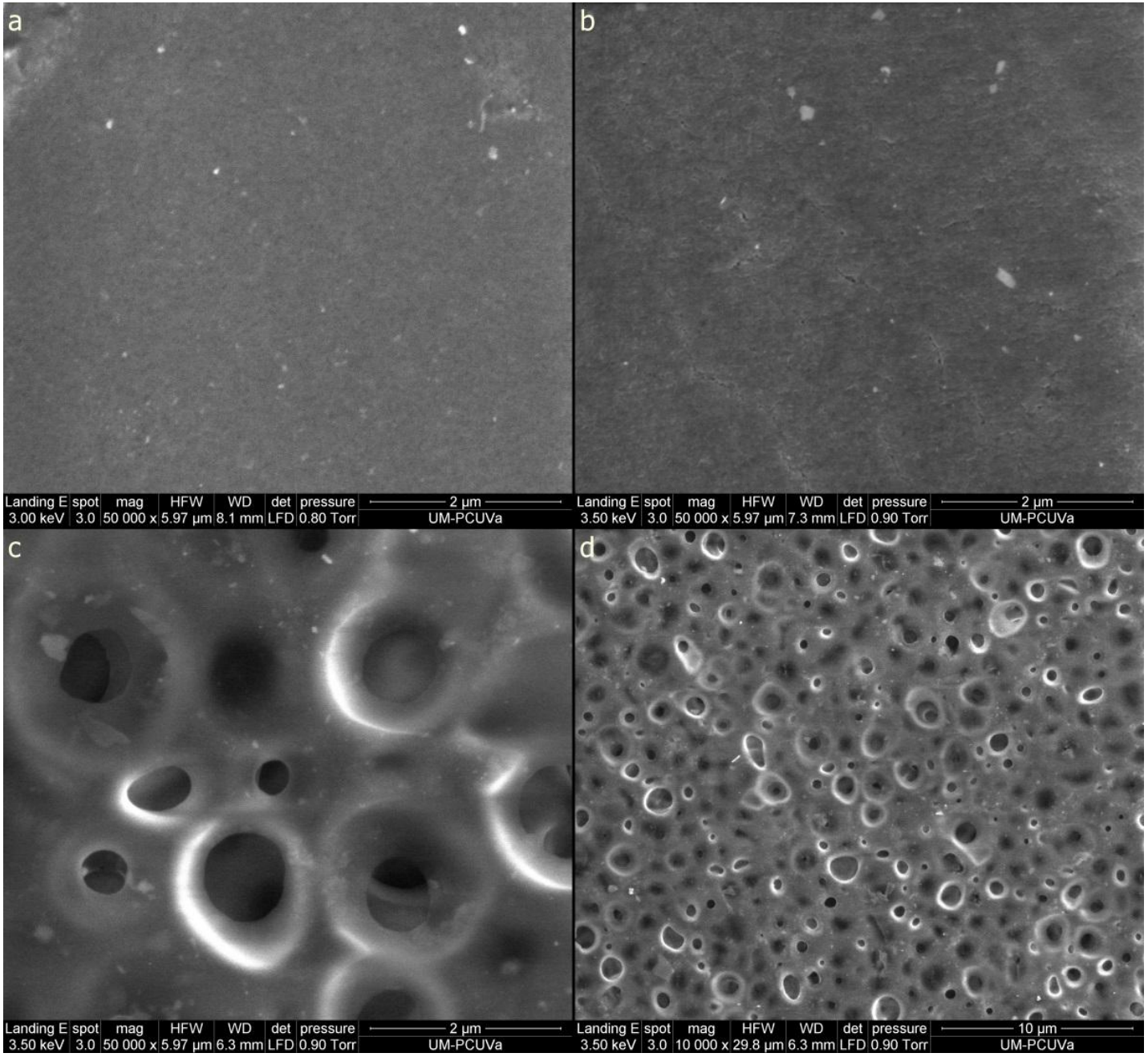

Fig. 6. SEM images of top surface of prepared membranes: (a) PES, (b) PES 0.025%SWCNT, (c, d) different magnifications of PES 0.5%SWCNT.

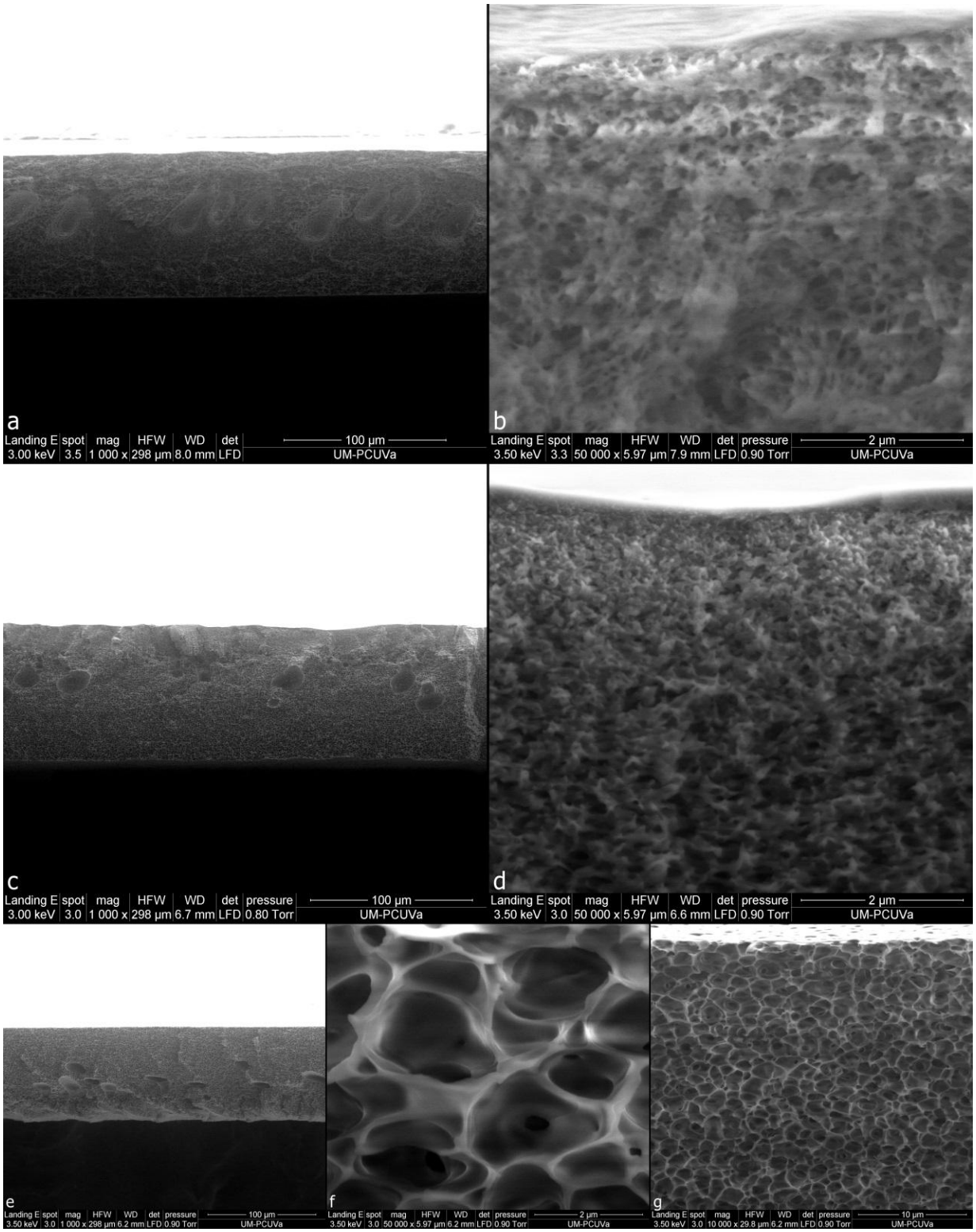

Fig. 7. SEM cross sectional images (different magnifications) of prepared membranes: (a, b) PES, (c, d) PES 0.025%SWCNT and (e,f,g) different magnifications of PES 0.5%SWCNT.

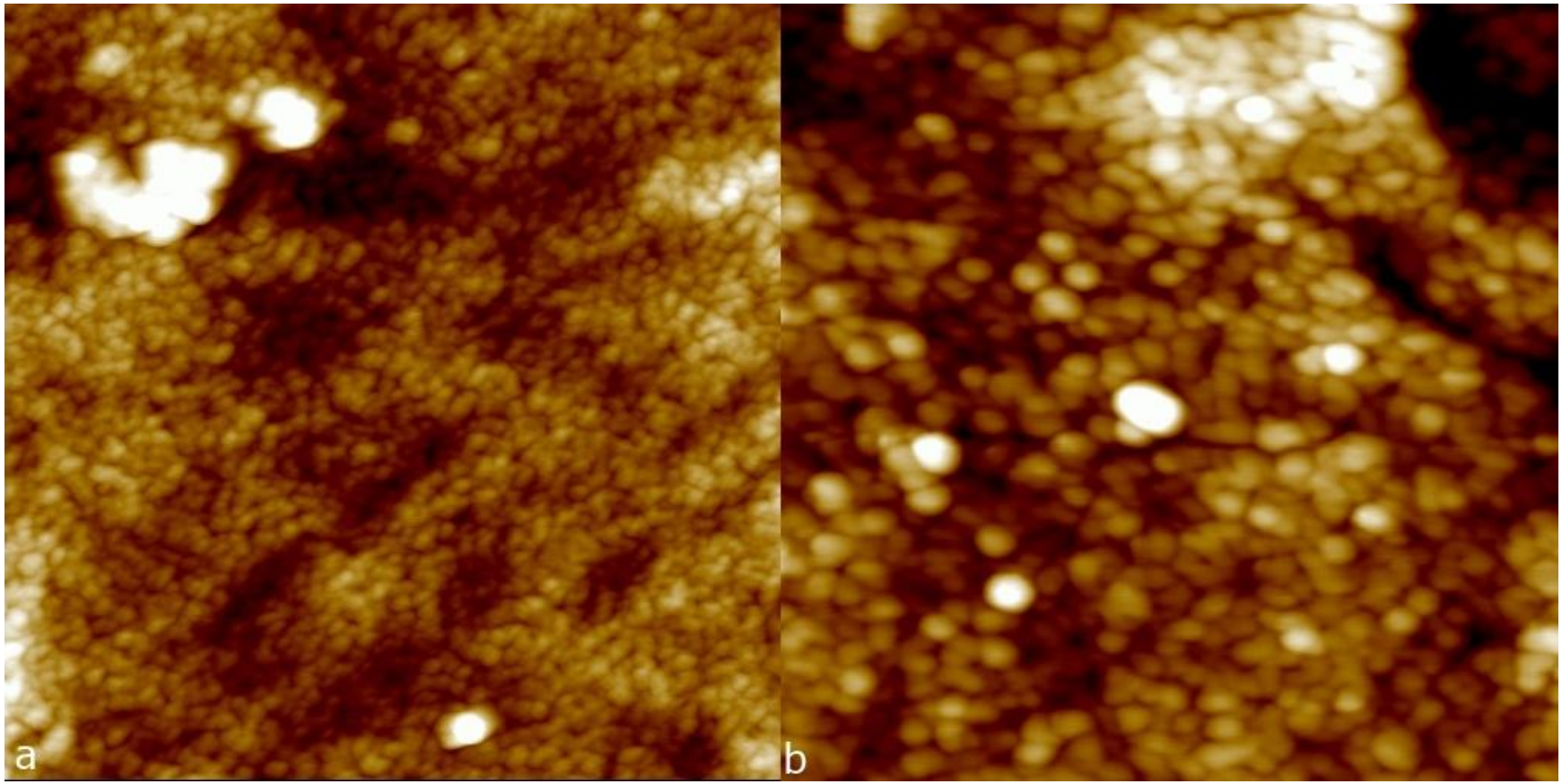

Fig. 8. AFM images of the surface of membranes: a - PES, b - PES 0.1%SWCNT. The size of the scanned areas is 1mmx1mm.

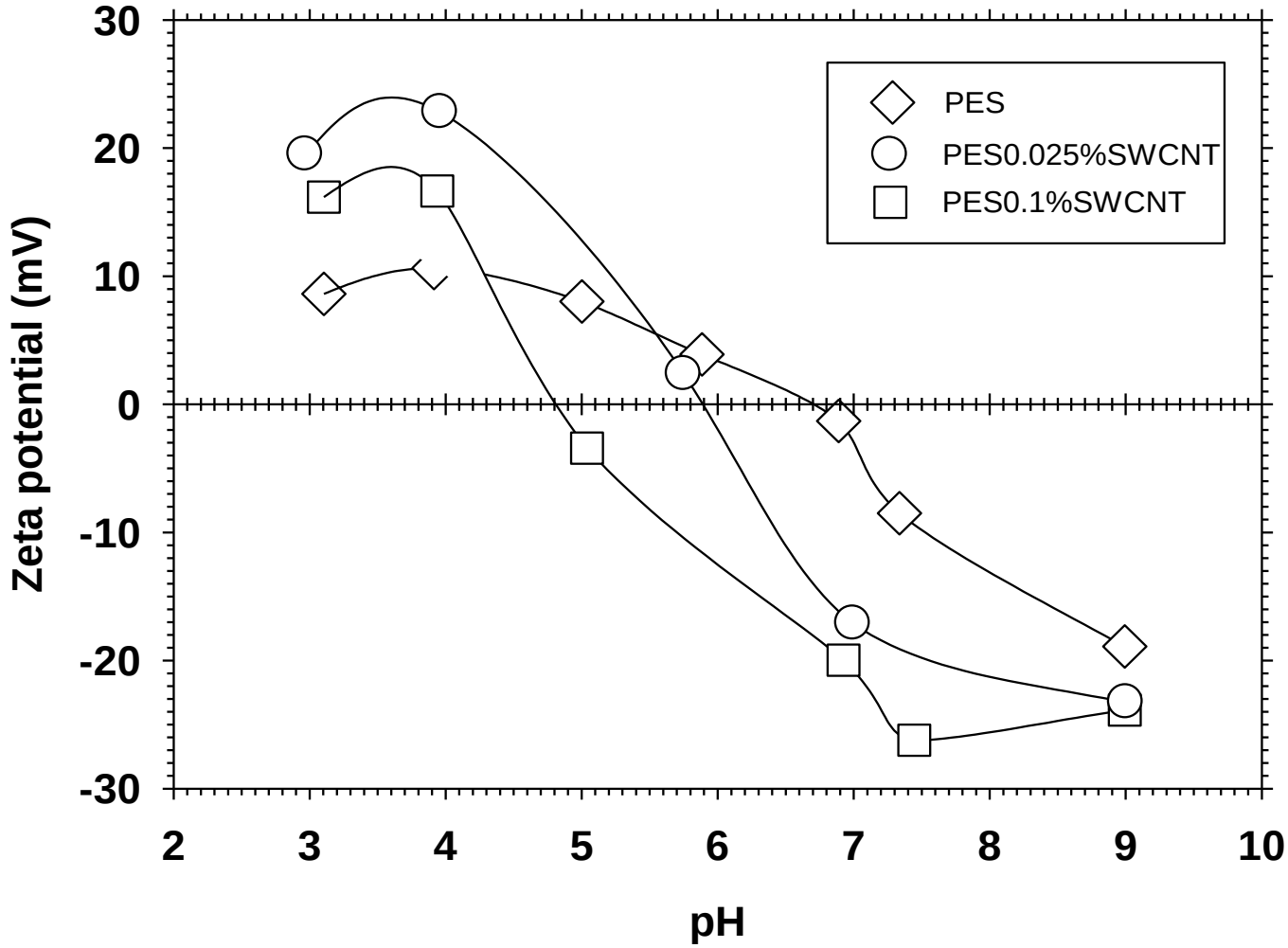

Fig. 9. Calculated zeta potential of the prepared membranes.

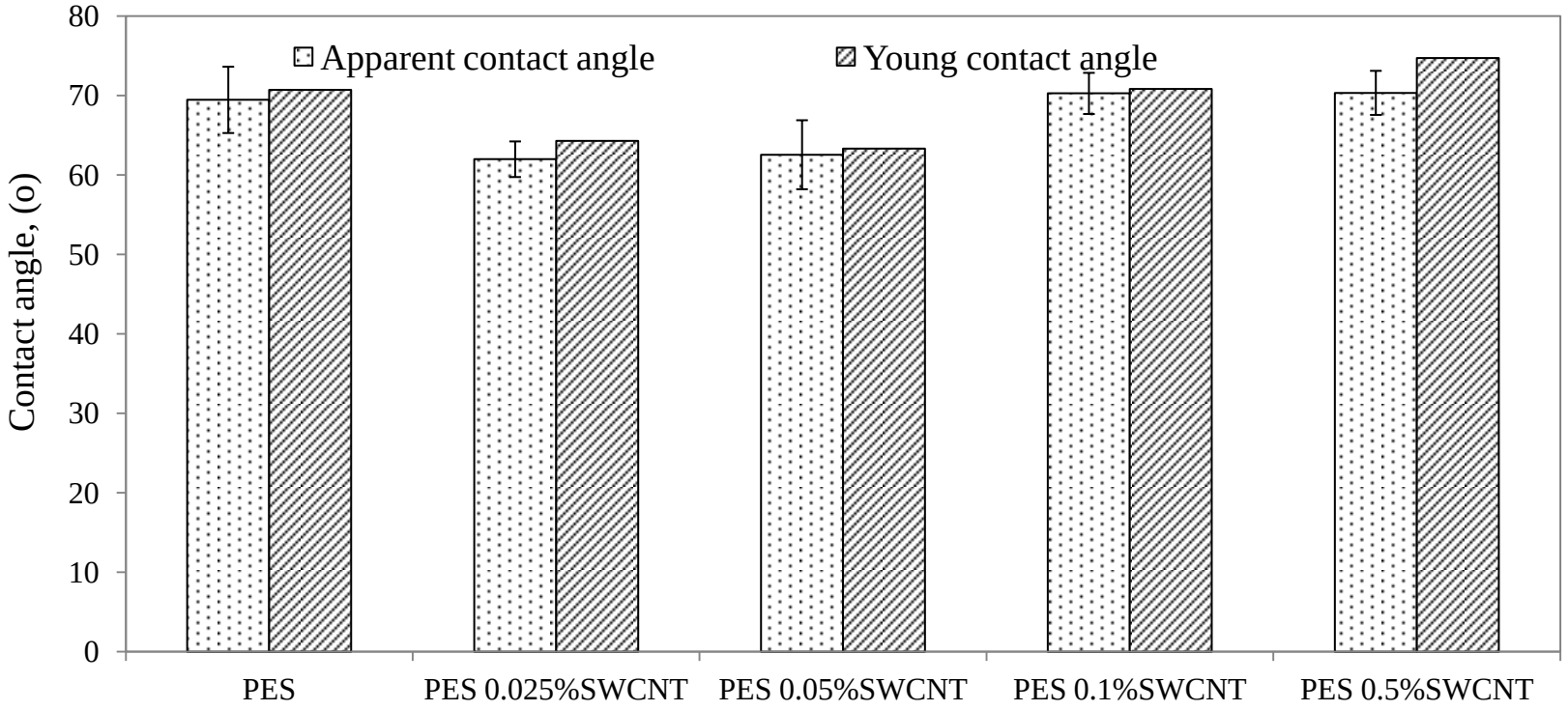

Fig. 10. Apparent and Young contact angle of prepared membranes as a function of SWCNT loading.

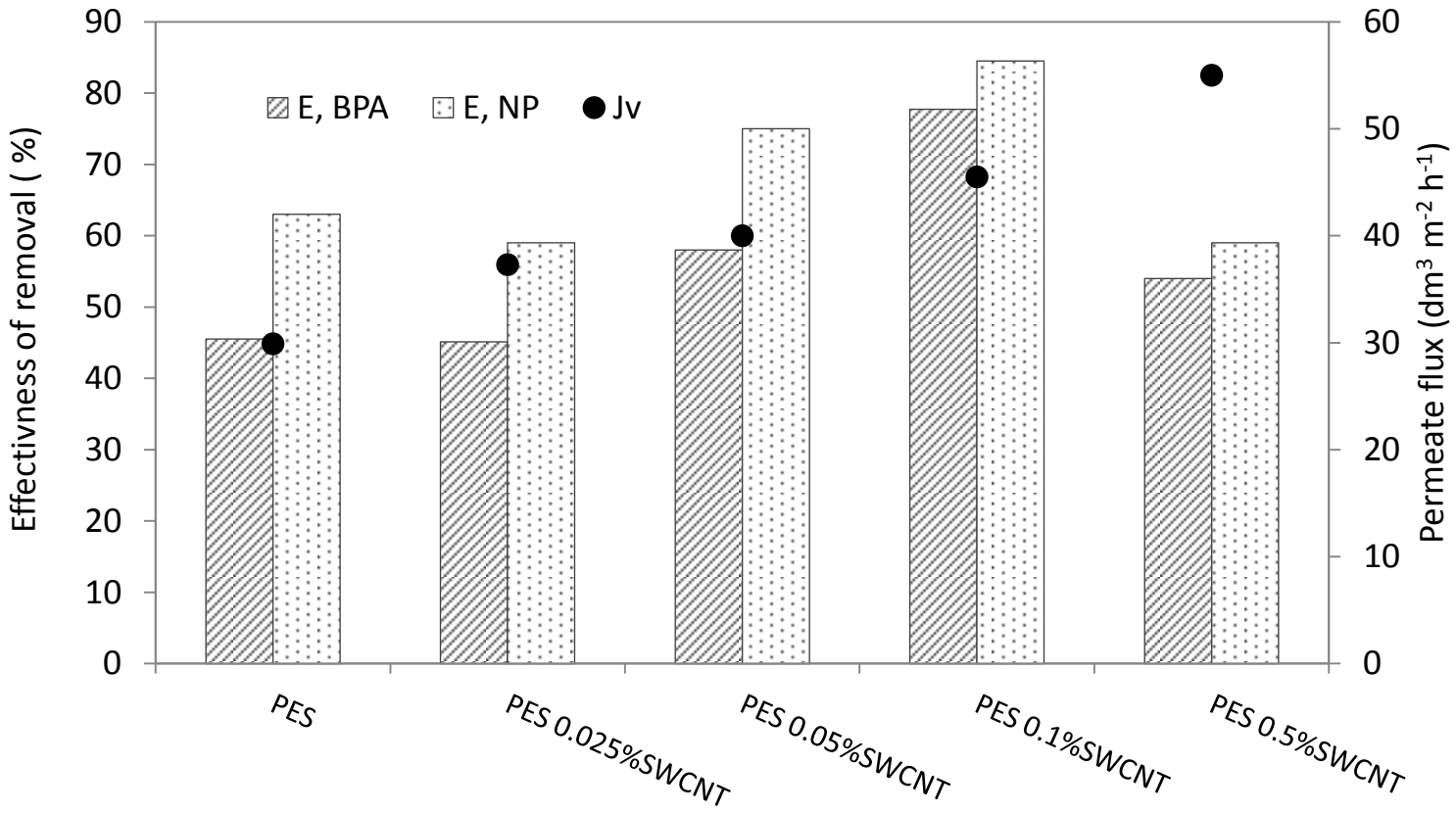

Fig. 11. Effect of SWCNT loading on wastewater permeability (at 0.5 bar) and on removal of micropollutants.

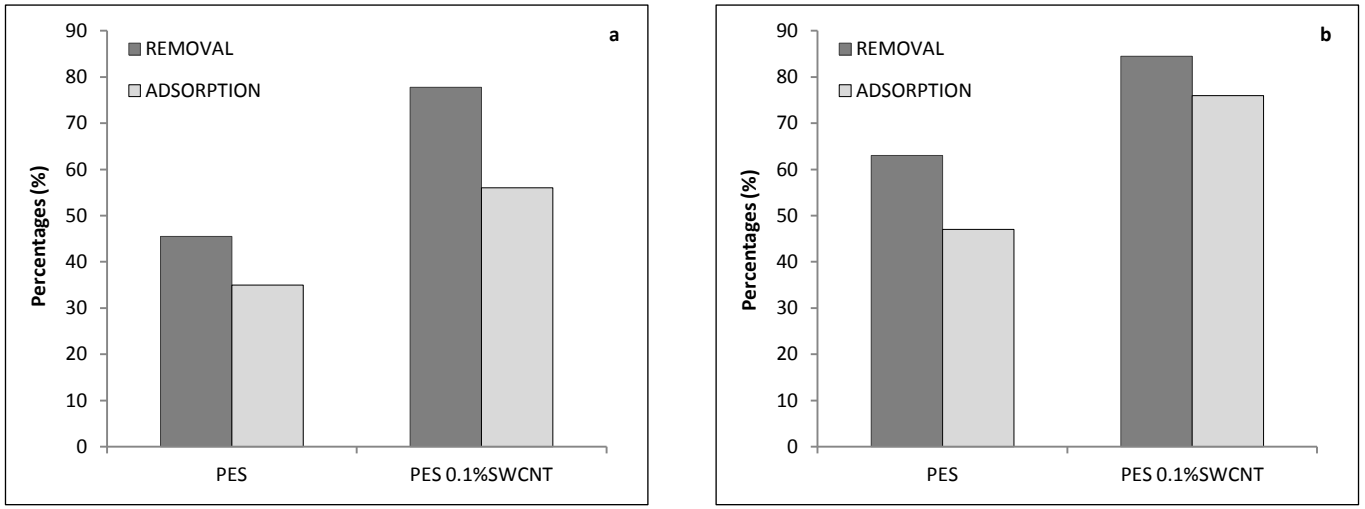

Fig. 12. Effectivenes of removal and adsorption of micropollutants: (a) BPA, (b) NP for selected membranes.

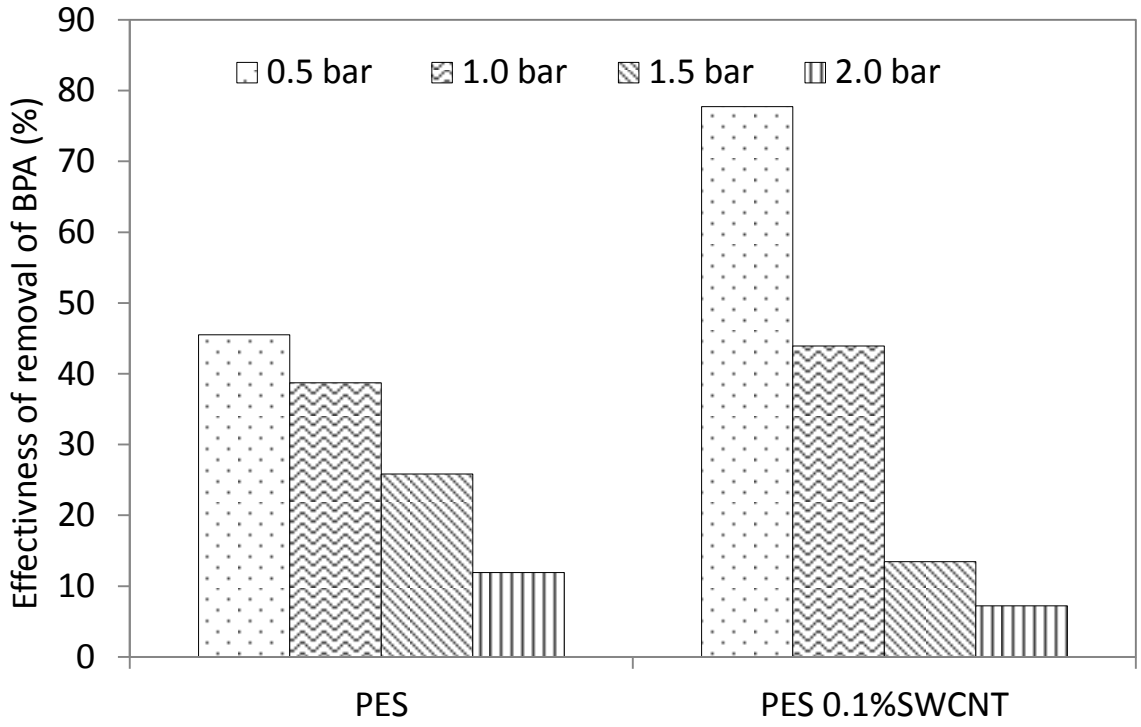

Fig. 13. Effect of transmembrane pressure on the effectiveness of removal of bisphenol A.

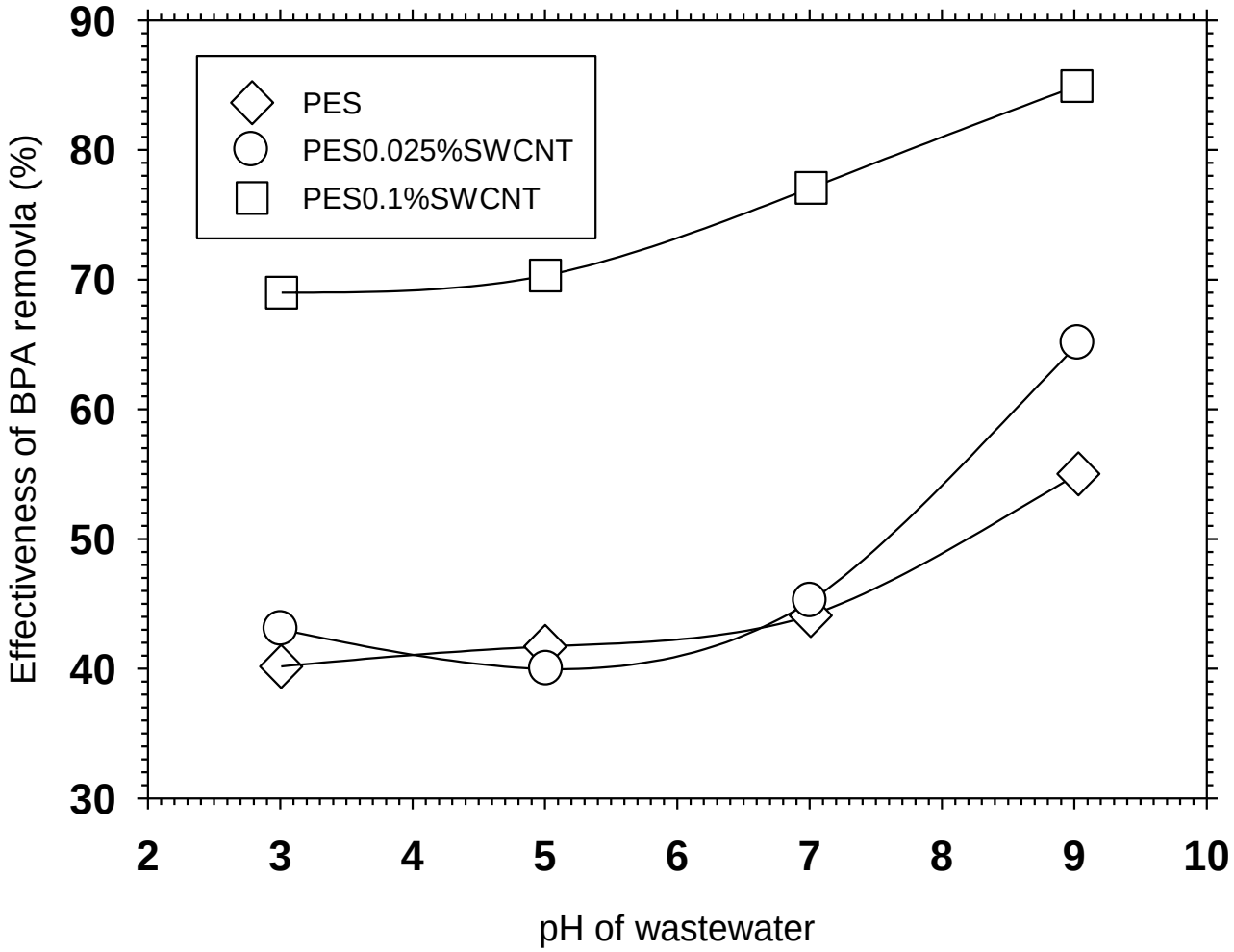

Fig. 14. Effect of the wastewater pH on the effectiveness of removal of BPA.

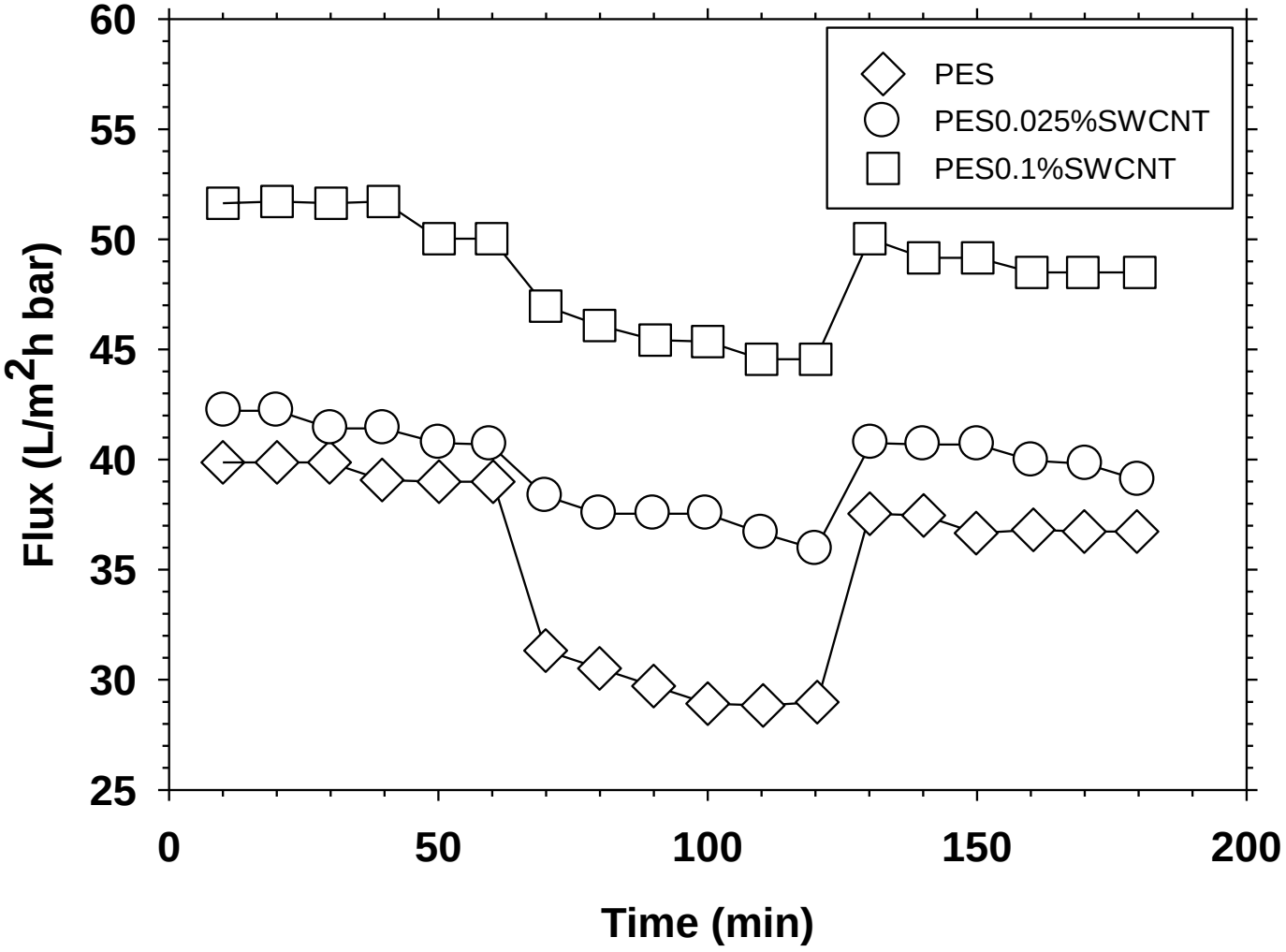

Fig.15. Different fluxes during filtration: Deionised water flux for pure membranes (0-60 min), wastewater flux (70-120 min) and deionised water flux after wastewater treatment (130-190 min).

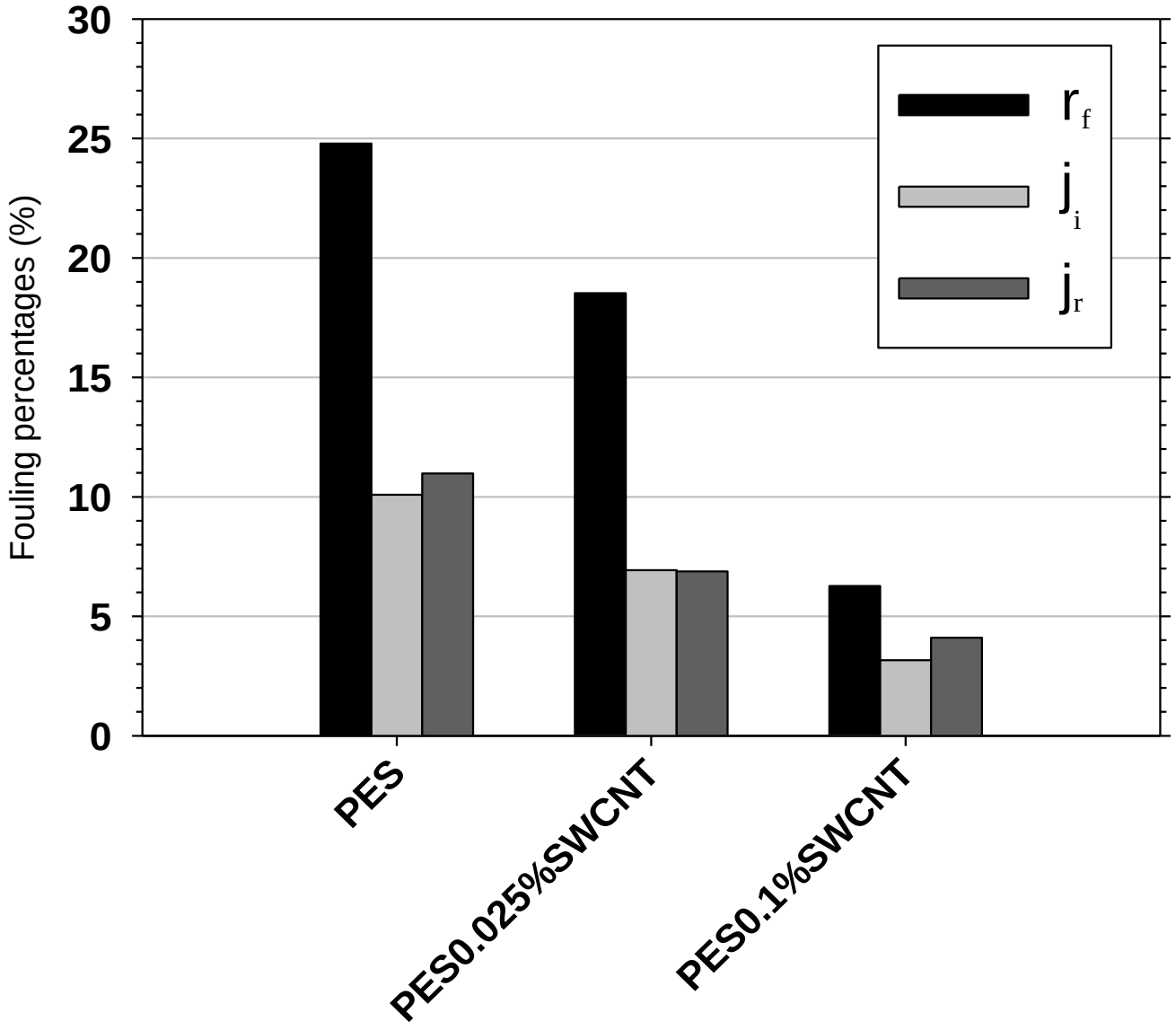

Fig. 16. Magnitude of the percentages defined in Equations (19) – (21) for some membranes.

TABLES

Table 1. Characteristics of nanotubes.

Symbol of carboxyl functionalized carbon nanotubes	Outer diameter (nm)	-COOH content (wt.%)	Length (μm)	Purity (%)
SWCNT	1-2	2.73	5-30	90

Table 2. Characteristics of compounds.

Compound	Molecular weight (g/mol)	Solubility in water (mg/dm^3)	Log K_{ow}	pKa	Stokes radius (nm)
Bisphenol A	228.29	120-200 (20-25 ^oC)	3.64	9.6-10.2	0.329
4-Nonylphenol	220.35	5.43(20 ^oC)	5.92	10.7-11.7	0.324

Table 3 Morphological parameters and MWCO for selected membranes from LLDP.

Membrane	Average radius Permeability (nm)	Average radius Pore number (nm)	MWCO (KDa)
PES	7.08	5.29	78.53
PES 0.025%SWCNT	6.59	6.02	72.55
PES 0.5%SWCNT	7.25	6.48	86.82

Table4. Average roughness of membranes measured in 1μmx1μm pictures.

Membrane	Average roughness R_a (nm)	Average Wenzel Index r_W (dimensionless)
PES	4.35	1.06
PES 0.025%SWCNT	6.01	1.08
PES 0.05%SWCNT	3.32	1.03
PES 0.1%SWCNT	3.83	1.03
PES 0.5%SWCNT	54.47	1.27

Table5. Different kinds of resistances and flux recovery for prepared membranes.

Membrane	R_m	R_f	R_c	R_{to}	F_R
	($10^{11} m^{-1}$)				(%)
PES	5.26	0.35	1.38	6.99	93.7
PES 0.025%SWCNT	5.02	0.16	0.40	5.58	96.8
PES 0.1%SWCNT	4.01	0.17	0.33	4.57	95.9